JOURNAL OF GEOPHYSICAL RESEARCH, VOL. 104, NO. B1, PAGES 993–1014, JANUARY 10, 1999

A degree 8 mantle shear velocity model from normal mode observations below 3 mHz

Joseph S. Resovsky and Michael H. Ritzwoller
Department of Physics, University of Colorado, Boulder

Abstract. We present inversions for a new three-dimensional mantle v_s model, MM2_L12D8, using a recently compiled catalogue of $\sim$ 2300 normal mode structure coefficients for 90 multiplets below 3 mHz. These inversions demonstrate the capabilities and limitations of existing normal mode data and reveal new images of structures in the midmantle (900-1800 km depth), which is poorly resolved by surface wave and body wave data. Our inversions are distinguished both by efforts to maintain consistency with a variety of seismic models, and hence data sets, and by attempts to characterize the sensitivity of our model to the choice of damping, to unspecified structures, and to data errors. We find that sensitivity to damping is the dominant source of model uncertainty, but MM2_L12D8 proves to be a robust model of v_s with amplitude uncertainties less than 35% for most depths and degrees. Other characteristics of MM2_L12D8 include χ^2 misfit to normal mode structure coefficients which is 58% smaller than that of the best existing models, greater similarity to existing models than they have to each other, perturbations relative to existing v_s models that are largest in the midmantle, and amplitudes that are most consistent with existing models that employ global, rather than local, basis functions. MM2_L12D8 also displays definite images of "slabs" and "plumes" in the midmantle and a spectrum of heterogeneity that is more continuous with depth than in most other models. These characteristics suggest that the midmantle participates in a very long wavelength pattern of circulation that involves at least the whole lower mantle. Inversions for v_p and ρ heterogeneities decorrelated from v_s structure demonstrate that there is a significant signal from such structures in the normal mode data, but v_p and ρ models are much more sensitive to damping than are v_s models. The normal mode catalogue must be expanded before normal mode models of v_p and ρ approach the reliability of the v_s structures in MM2_L12D8. (This model, together with our catalogue of structure coefficients, is available at web site phys-geophys.colorado.edu/geophysics/nm.dir.)

1. Introduction

1.1. Motivation

This paper describes inversions of a catalogue of normal mode structure coefficients below 3 mHz for a degree 8 model of shear velocity structure in the mantle. There are three motivations for this study. First, there are significant discrepancies among mantle v_s models, even at the longest wavelengths. These structural differences include the amplitude and geometry of dynamically important features such as "slabs" and "plumes" in the lower mantle. Second, recent normal mode measurements are particularly sensitive to structures in the midmantle (900-1800 km depth), where the resolution provided by body wave and long-period surface wave data is poorest [*Masters et al.*, 1996] and where discrepancies among existing models are largest. Several new sets of normal mode structure coefficients [*Tromp and Zanzerkia*, 1995; *He and Tromp*, 1996; *Resovsky and Ritzwoller*, 1998] have been compiled since previous efforts to model mantle structure with normal modes [e.g., *Ritzwoller et al.*, 1988; *Li et al.*, 1991; *Widmer et al.*, 1992]. Third, existing shear velocity models exhibit unsatisfactory misfits to normal mode structure coefficients sensitive to the midmantle. We need to understand what these misfits tell us about the Earth as well as the extent to which they can be reduced by reasonable modifications to existing models.

Paper number 1998JB900025.
0148-0227/99/1998JB900025$09.00

1.2. Comparisons of Existing Earth Models

Existing mantle models have been constructed using different input data, different inversion regularization and damping schemes, different structural parameterizations, and different theoretical bases. These differ-

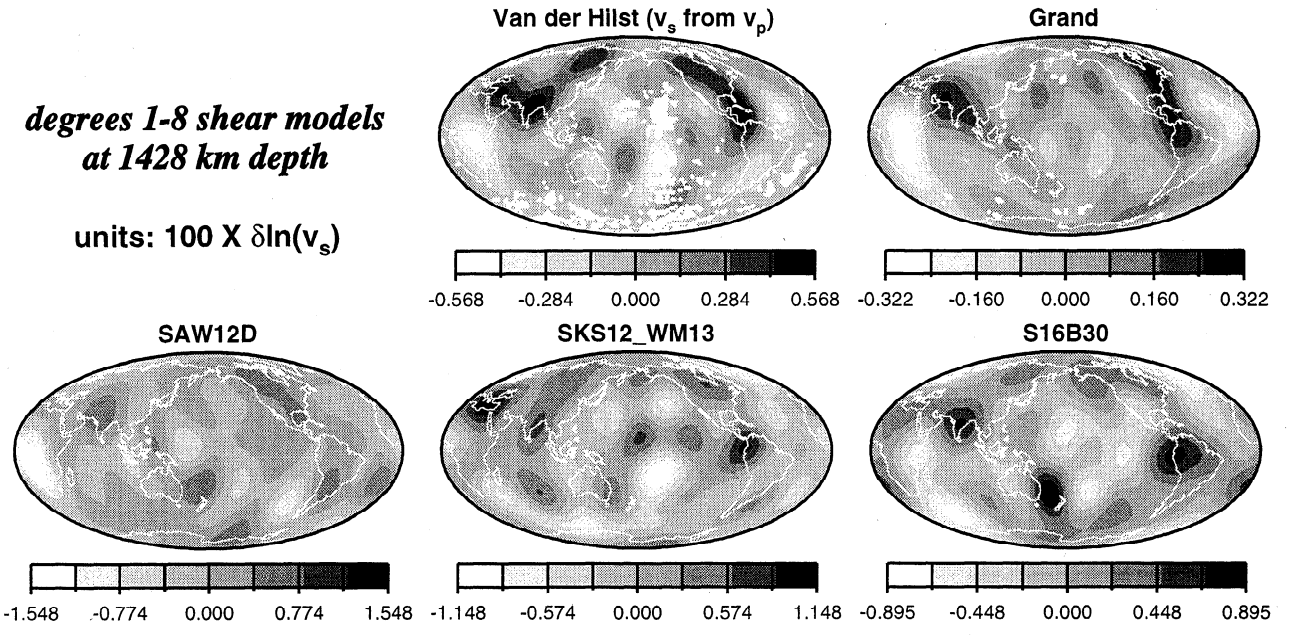

Figure 1. Degree 1-8 spherical harmonic components of shear velocity models in the midmantle. Units are percent shear velocity perturbation. The model of Van der Hilst has been converted from $d\ln v_p$ to $d\ln v_s$ using $d\ln v_p/d\ln v_s = 0.5$. Blank spots in the Van der Hilst and Grand models indicate unmodeled regions. The models of Van der Hilst and Grand are "local basis function" (LBF) models. The others are "global basis function" (GBF) models.

ences lead to sizable discrepancies among the models [*Ritzwoller and Lavely*, 1995], particularly in the midmantle, where the resolution provided by body waves and surface waves is poor. Such discrepancies are visible in Figure 1, which shows five recent models at a single midmantle depth.

The bottom three maps of Figure 1 show the spherical harmonic degrees 1-8 components of the models SAW12D [*Li and Romanowicz,* 1996], SKS12WM13 [*Liu and Dziewonski*, 1994], and S16B30 [*Masters et al.,* 1996]. These are all examples of models that represent structure using global basis functions (GBFs), which are combinations of spherical harmonics and polynomial functions of radius. Other recent models using GBFs include those of *Masters et al.* [1992], *Su and Dziewonski* [1994], and *Liu* [1997]. Figure 1 also displays the models of *Van der Hilst et al.* [1997] and *Grand et al.* [1997] (hereinafter referred to as the Van der Hilst model and the Grand model). These two models parameterize structure with local basis functions (LBFs) in which the Earth is divided into regions of constant velocity with dimensions of a few hundred kilometers. The degree 1-8 maps of the LBF models in Figure 1 result from degrees 0-16 spherical harmonic decomposition of the original models. Other models that employ LBFs include those of *Widiyantoro et al.* [1997] *Bijwaard et al.* [1998], and *Vasco and Johnson* [1998].

Except for the v_p model of Van der Hilst, the midmantle models in Figure 1 are dominantly constrained by recordings of shear waves which travel through the lower mantle. The three GBF models display considerable discrepancies, even at the long wavelengths shown here. At the depth displayed in Figure 1, they are not consistent in overall amplitude, in the relative amplitudes of the various high-velocity anomalies, or in the location of low-velocity "plumes." There are even larger differences between models with GBF and LBF parameterizations. The LBF shear velocity model of Grand has much smaller amplitudes for midmantle structure than the GBF models, and is characterized by extended high-velocity features that are noticeably more "slab-like" than corresponding features in the GBF models.

Discrepancies between the Grand and Van der Hilst models are also worth noting, even though the latter model is constrained only by P wave travel times. The midmantle results of other recent inversions [e.g., *Giardini et al.*, 1987, 1988; *Li et al.*, 1991; *Robertson and Woodhouse*, 1996] are reasonably consistent with v_s and v_p structures that are perfectly correlated, subject to a scaling factor $\alpha = d\ln v_p/d\ln v_s$ with $0.4 < \alpha < 0.8$. However, correlation between the two LBF models in the lower mantle is neither better nor worse than correlation among GBF models of shear velocity. Although both LBF models display lower mantle "slab remnants" in Figure 1, they manifest different patterns of high-velocity anomalies under southern and eastern Asia. Like the Grand model, the Van der Hilst model has significantly smaller midmantle amplitudes than the GBF models, unless $d\ln v_p/d\ln v_s < 0.3$. Conversely, to give the two LBF models similar amplitudes would require a scaling of $d\ln v_p/d\ln v_s > 0.9$.

Figure 2 quantifies differences in both amplitude and geometry of existing models, using comparisons of pairs of models as functions of radius. In much of the man-

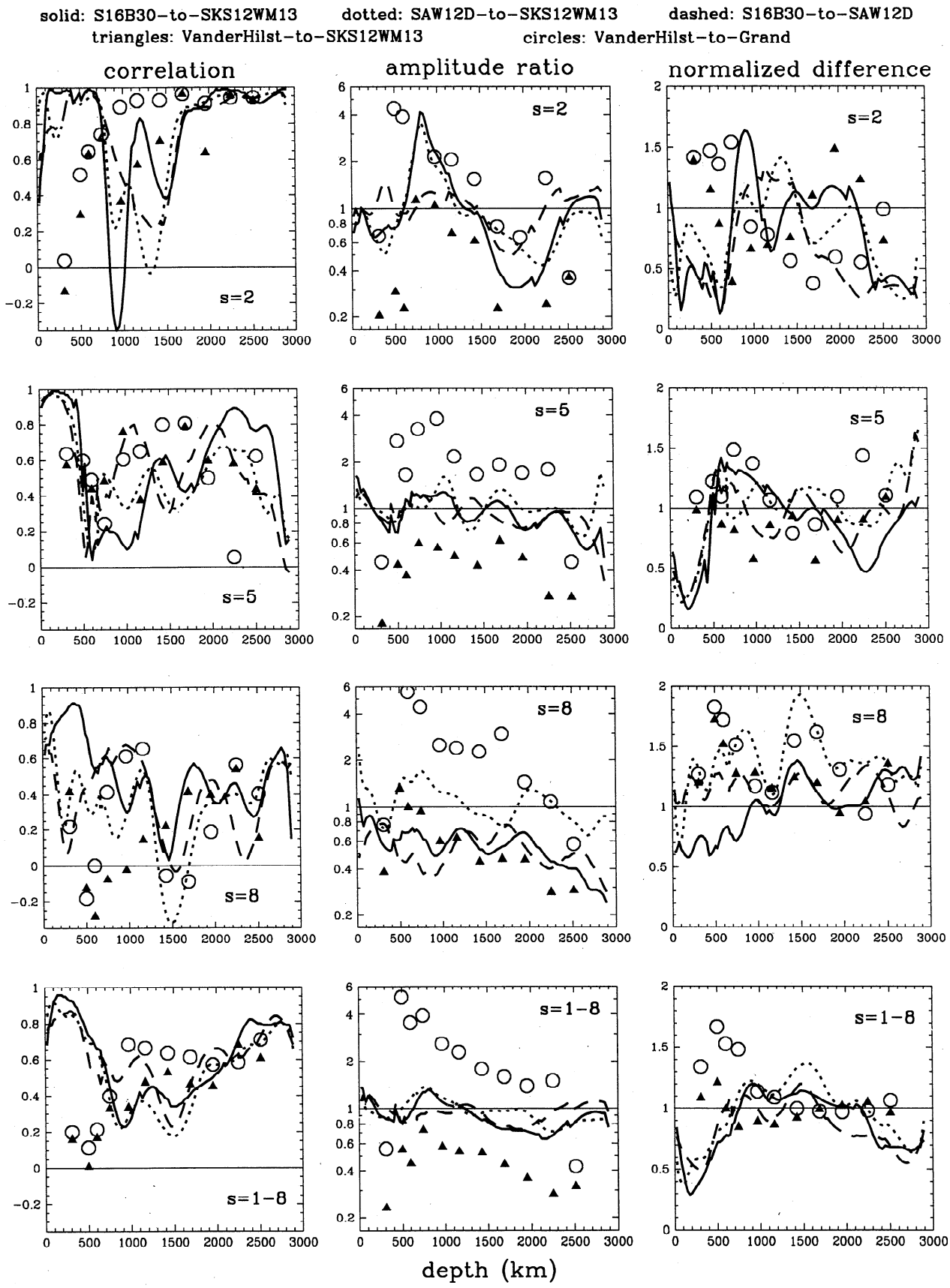

Figure 2. Radial comparisons of mantle models. Five pairs of models are compared at degrees (top to bottom) 2, 5, and 8, and 1-8 combined. (left) Geographic correlation at each depth. (middle) Ratio of RMS amplitudes at each depth. (right) RMS amplitude of the difference between models normalized by the average of the RMS amplitudes of the models S16B30, SKS12WM13, and SAW12D at each depth, except for the Grand-Van der Hilst difference, which is normalized by the average amplitudes of those two models.

tle, and particularly in the midmantle, sizable differences exist between most pairs of models at most degrees of structure. Even at degree 2, model correlations are lower than 60% and amplitudes differ by factors of 2 or more in the midmantle. The largest discrepancies are amplitude differences between GBF and LBF models. In general, the differences between models in the midmantle are of about the same size as the structures represented by the models themselves.

1.3. The Normal Mode Catalogue

Our catalogue of normal mode structure coefficients has been produced by applying the generalized spectral fitting (GSF) technique to the analysis of normal mode multiplets in long-period seismic spectra [*Resovsky and Ritzwoller*, 1998]. GSF incorporates coupling between nearby multiplets. GSF analyses are distinguished from other recent normal mode studies [e.g., *Tromp and Zanzerkia*, 1995; *He and Tromp*, 1996] by this explicit incorporation of coupling, by the specification of structure coefficients at degrees beyond 6, and by the use of data from a relatively large number of strong earthquakes. New measurements include the first normal mode coefficients for odd-degree structure [*Resovsky and Ritzwoller*, 1995], coefficients for several multiplets not previously analyzed, and coefficients through structural degree 12 for some multiplets [*Ritzwoller and Resovsky*, 1995]. In addition, structure coefficient error estimates have been obtained using Monte Carlo simulations of the effects of theoretical errors and of noise in the data. For these reasons, our normal mode catalogue is significantly refined relative to the collections of normal mode data incorporated in models such as S16B30 or SH.10c.17 [*Masters et al.*, 1992]. (The catalogue is available through our web site at physgeophys.colorado.edu/geophysics/nm.dir.)

To assess existing models, we compare the catalogued normal mode structure coefficients to those predicted by the models. Table 1 gives the results of such comparisons using the misfit statistic χ defined by

$$\chi = \left[\frac{1}{K} \sum_{k=1}^{K} \frac{(c_k^{\mathtt{model}} - c_k)^2}{\sigma_k^2} \right]^{1/2}, \qquad (1)$$

where K is the number of catalogued structure coefficients (c_k) for a particular structural degree and/or mode branch and σ_k is the uncertainty estimate for each coefficient. The overall misfit of each existing model is worse than $\chi = 2.4$ ($\chi^2 \cong 6.0$), which implies that individual coefficients are often misfit by more than twice the estimated uncertainty. Furthermore, the greatest misfits produced by most models are for coefficients along the ${}_1S$ overtone branch, which is dominantly sensitive to lower mantle shear velocity, and those of the ${}_0S$ branch, which dominantly samples shear structure in the transition zone and outermost lower mantle. These observations suggest that a significant portion of the unfit normal mode signal results from poorly modeled long-wavelength shear velocity structures in the transition zone and midmantle.

1.4. Focus of This Investigation

This investigation attempts to answer two questions. The first is: How much can we improve fit to our catalogue of normal mode structure coefficients with mantle models that are both robust and plausible? We seek to identify models which are "robust" in the sense that uncertainties in the estimated structures are much smaller than the structures themselves. To do so, we estimate the uncertainties in normal mode models of v_s, v_p, and ρ associated with effects such as indefinite choices of inversion damping (sections 2.4 and 3.4.1) and errors inherent in the data. We also seek models which are "plausible" in the sense that the structures described are consistent with the other forms of seismic data. Because acquiring and incorporating these very large data sets would require prohibitive efforts, we use a proxy for consistency with other seismic data: consistency with the models constructed to fit these data. In particular, we require that our new models lie "between" existing models (section 2.3). This strategy clearly is not optimal, and we hope that this study will motivate other researchers to use normal mode structure coefficients in inversions with other types of data.

Our second question is: What do robust and plausible models that fit normal mode data reveal about mantle structure, particularly in the heretofore poorly constrained midmantle? To answer this question, we use comparisons with existing mantle models. Such comparisons identify the important features of our normal mode models and indicate the extent to which normal modes discriminate between the differing midmantle amplitudes of GBF and LBF models, between the differing geometries of midmantle "slab remnants," and between the different paths of "plumes" through the lower mantle.

2. Method

Normal mode structure coefficients are linear functionals of three-dimensional (3-D) Earth structure, as described in section 2.1 below. For this reason the subset of structure coefficients at each spherical harmonic degree and order is readily employed in linear inversions for the corresponding structure as a function of depth. However, structure coefficients alone provide imperfect resolution of mantle structure. To maintain consistency with existing models, it is necessary to apply several constraints derived from a priori assumptions about mantle structures. These include parameterization of the models (section 2.2), damping which keeps the output models near to the input models (section 2.3), and damping which reduces amplitude instabilities (section 2.4).

Table 1. Misfit of Model Predictions to Normal Mode Structure Coefficients

Mode Branch	χ Misfit[a] at Each Structural Degree s							
	$s=1$	$s=2$	$s=3$	$s=4$	$s=5$	$s=6$	$s=8$	$s=[1-8]$
				Model MM2_L12D8				
${}_0S$	-	1.71	-	1.46	-	1.37	1.14	1.37
${}_0T$	-	1.99	-	1.40	-	1.47	1.45	1.55
${}_1S$	-	2.66	-	1.19	-	1.23	1.25	1.65
${}_1T$	-	2.09	-	1.93	-	-	-	2.01
${}_2S$	-	3.03	-	1.39	-	1.47	-	1.82
${}_4S_{,5}S$[b]	-	3.42	-	2.23	-	1.84	1.05	2.36
all	1.67	2.31	2.28	1.53	1.33	1.47	1.25	1.65
				Model SKS12WM13				
${}_0S$	-	4.78	-	3.43	-	2.25	2.23	2.99
${}_0T$	-	2.32	-	1.41	-	1.61	1.60	1.69
${}_1S$	-	4.26	-	3.17	-	2.06	2.00	2.97
${}_1T$	-	2.40	-	2.13	-	-	-	2.27
${}_2S$	-	3.73	-	1.51	-	1.57	-	2.10
${}_4S_{,5}S$	-	4.66	-	2.83	-	1.93	1.29	3.02
all	1.87	3.58	3.46	2.46	2.61	1.95	2.00	2.52
				Model S16B30				
${}_0S$	-	3.86	-	3.61	-	2.06	1.71	2.70
${}_0T$	-	3.81	-	1.50	-	1.53	1.62	2.10
${}_1S$	-	5.72	-	2.37	-	1.59	1.87	3.19
${}_1T$	-	2.44	-	2.08	-	-	-	2.26
${}_2S$	-	3.63	-	1.60	-	1.53	-	2.08
${}_4S_{,5}S$	-	3.40	-	2.55	-	1.97	1.22	2.49
all	3.21	3.76	2.89	2.44	2.37	1.80	1.68	2.47
				Model SAW12D				
${}_0S$	-	6.47	-	2.61	-	2.78	2.11	3.30
${}_0T$	-	2.28	-	1.71	-	1.64	1.49	1.74
${}_1S$	-	5.19	-	1.87	-	1.98	1.96	2.97
${}_1T$	-	2.49	-	1.76	-	-	-	2.16
${}_2S$	-	4.99	-	1.41	-	1.58	-	2.50
${}_4S_{,5}S$	-	2.46	-	2.41	-	2.02	1.45	2.19
all	3.08	4.31	2.90	2.02	1.96	2.19	1.89	2.63
				Number of Multipets and Coupling Pairs; Number of Coefficients				
${}_0S$	-	19;95	-	17;153	-	16;208	14;28	19;725
${}_0T$	-	19;95	-	17;153	-	11;143	8;136	19;567
${}_1S$	-	10;50	-	7;63	-	5;65	3;51	10;229
${}_1T$	-	9;45	-	5;45	-	-	-	9;90
${}_2S$	-	10;50	-	10;90	-	10;130	-	10;283
${}_4S_{,5}S$	-	6;30	-	4;36	-	3;39	1;17	6;122
all	3;9	87;435	3;21	74;666	7;77	50;650	26;442	100;2290

[a] $\chi = \left[\sum_{k=1}^{K}(c_k^{\text{model}} - c_k)^2/\sigma_k^2 K\right]^{1/2}$.
[b] Modes dominantly sensitive to lower mantle v_p.

2.1. Structure Coefficients

For each spherical harmonic component of structure, with degree s and order t, and for each multiplet or coupling pair of multiplets, referred to with index k, there is a structure coefficient:

$$ {}_k c_s^t = \int_0^{r_E} d\ln \mathbf{m}_s^t(r) \cdot {}_k\mathbf{M}_s(r) r^2 dr + \sum_d h_{sd}^t \, {}_k D_{sd} r_d^2; \quad (2) $$

where

$$ d\ln \mathbf{m}(r) = \frac{\delta \mathbf{m}(r)}{\mathbf{m}(r)} = [d\ln v_p(r), d\ln v_s(r), d\ln \rho(r)] \quad (3) $$

represent relative perturbations to a 1-D model (usually the preliminary reference Earth model of *Dziewonski and Anderson*, 1981); h_d are perturbations to the location of discontinuities at radii r_d of the 1-D model;

and $\mathbf{M}(r)=[P(r),S(r),R(r)]$ and D_d are known structure kernels and boundary factors. The kernels for v_s, v_p, and ρ can be derived from those for κ, μ, and ρ provided by *Woodhouse* [1980].

2.2. Model Parameterization

The starting models for our inversions are all globally parameterized models in which lateral variations in v_s, v_p, and ρ are assumed to be perfectly correlated. This assumption implies scaling relations of the form $d\ln v_p(r) = \alpha(r) d\ln v_s(r)$ and $d\ln \rho(r) = \beta(r) d\ln v_s(r)$ for some radial functions $\alpha(r)$ and $\beta(r)$. For this study we usually employ $[\alpha(r),\beta(r)] = [0.8, 0.3]$ in the upper mantle and $[0.5, 0.2]$ in the lower mantle. The upper mantle value for α is the commonly employed result from *Anderson et al.* [1968], and the lower mantle value is consistent with the results of *Li et al.* [1991]. We have also performed inversions using smaller values for α near the top and bottom of the mantle (section 3.4.2), such as may be associated with partial melts. The values for β are consistent with the mineralogical results of *Karato* [1993] and were used, for example, in the geoid inversions of *Thoraval and Richards* [1997].

In most of our inversions we maintain the assumption of scaling between v_s, v_p, and ρ, because breaking the scaling relations has a relatively weak effect on the character of our v_s models (section 3.4.2). In addition it is impractical to estimate v_s, v_p, and ρ simultaneously using the present normal mode catalogue, because models of v_p and ρ are much more sensitive to indefinite choices of inversion damping than are v_s models. With the scaling relations in effect, and if we also choose to ignore boundary perturbations, (2) can be rewritten:

$$c_k = \int_0^{r_E} M_k(r)\, \delta\hat{v}(r) dr, \tag{4}$$

where the $\delta\hat{v} \equiv \delta v_s$ and the scalar kernel is $M(r) = [S(r)+\alpha(r)P(r)+\beta(r)R(r)]\, r^2/v_s(r)$. We have dropped the s and t indices because we can consider a single spherical harmonic component of structure in each inversion. Because our model is a perturbation to a 3-D input model, we replace $\delta\hat{v}$ with $v_{\mathtt{IN}} + \delta v$, where $v_{\mathtt{IN}}$ is an input 3-D model which yields structure coefficients ${}_kc^{\mathtt{IN}}$. With $\Delta c_k^{\mathtt{IN}} = c_k - c_k^{\mathtt{IN}}$, we have

$$\Delta c_k^{\mathtt{IN}} = \int_0^{r_E} M_k(r)\, \delta v(r) dr. \tag{5}$$

Because structure coefficients are coefficients of GBFs, we use GBFs for the lateral parameterization of our models and GBF models SKS12WM13, SAW12D, and S16B30 as inputs. These input models have three different radial parameterizations. Our own parameterization of $\delta v(r)$ is a simple layerization, which appears to be an adequate compromise. We assume that we have L layers with index l, bounded by $[r^l_{\mathtt{min}}, r^l_{\mathtt{max}}]$, in which $\delta v(r^l_{\mathtt{min}} < r < r^l_{\mathtt{max}}) = \delta v_l$. With

$$M_{kl} = \int_{r^l_{\mathtt{min}}}^{r^l_{\mathtt{max}}} M_k(r)\, dr\,, \tag{6}$$

equation (5) becomes

$$\Delta c_k^{\mathtt{IN}} = \sum_{l=1}^{L} M_{kl} \delta v_l\,. \tag{7}$$

We use 12 layers, 9 in the lower mantle and 3 in the upper mantle. The bottom and top depths of these layers, in kilometers, are [(2891, 2643), (2610, 2380), (2347, 2117), (2084, 1822), (1789, 1559), (1526, 1296), (1264, 1067),(1034, 870), (837, 670), (670, 400), (400, 220), (220, 24)]. These depths all correspond to radial knots of the *Dziewonski and Anderson* [1981] model.

To find the perturbations to $v^{\mathtt{IN}}$ which fit coefficients c_k that have corresponding uncertainty estimates σ_k, we invert the matrix equation

$$\mathbf{M}' \cdot \delta\mathbf{v} = \mathbf{\Delta c}'\,, \tag{8}$$

where $M'_{kl} = M_{kl}/\sigma_k$ and $\Delta c'_k = \Delta c_k^{\mathtt{IN}}/\sigma_k$, subject to the damping described in sections 2.3 and 2.4.

2.3. Damping to Enforce Consistency With Existing Models

As discussed in section 1.4, we attempt to ensure that these inversions produce models that are consistent with other seismic data by requiring that the output models remain relatively close to a set of existing models. There are two steps to enforcing this requirement. The first is weighting and damping such that, in any given layer, an output model differs from an input model no more than existing GBF models differ from each other. The second is damping that further confines output models to the space "between" existing models.

We damp the outputs of normal mode inversions to be close to input models using a weighting defined by the differences between existing models. Given a pair of existing models v_A and v_B (usually SKS12WM13 and S16B30), we find the average RMS amplitude of the two models within each layer $\overline{v_l}$, the average RMS difference between the two models $v_l^{\mathtt{dif}}$, and the relative difference $v_l^{\mathtt{rdif}} = v_l^{\mathtt{dif}}/\overline{v_l}$. We define a diagonal matrix $\mathbf{W}$ of layer weights

$$W_{ll} = w_l / v_l^{\mathtt{rdif}}\,, \tag{9}$$

where the w_l are ad hoc adjustments to the relative difference weighting. The $1/v_l^{\mathtt{rdif}}$ factors are plotted in Figure 3a. The smallest values (weakest damping) correspond to layers where relative differences between existing models are large. Thus our models are most free to differ from the input models at depths and degrees where relatively large differences among existing models imply that other forms of seismic data do not provide strong constraints on mantle structure. Conversely, in the uppermost mantle, where existing models are most similar, our models are relatively strongly damped. We

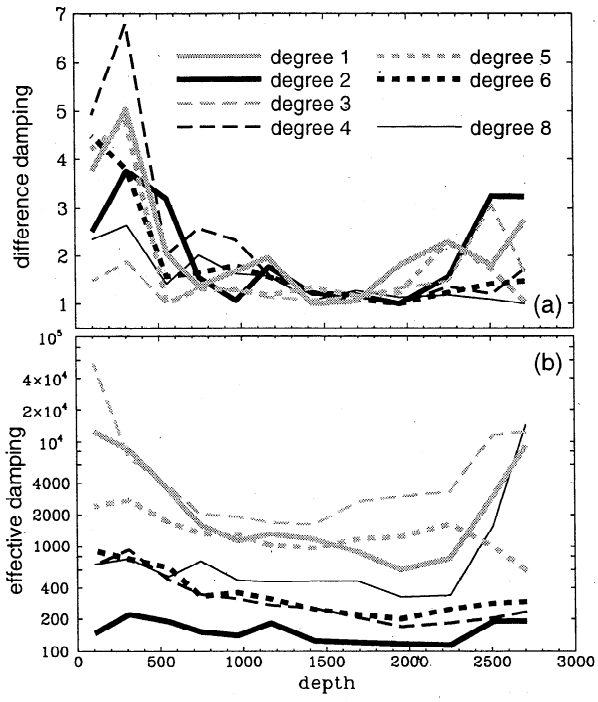

Figure 3. (a) Difference damping factors, $1/v_l^{\mathrm{rdif}}$, as defined in section 2.3, plotted as a function of layer depth for each structural degree. The models used to compute v_l^{rdif} are SKS12WM13 and S16B30. (b) Effective damping strength as a function of layer depth for each structural degree. Effective damping at each degree is defined as the adjusted damping, $\lambda_1 W_{ll}$ (equations (9) and (10)), divided by the number of modes N inverted at that degree (see Table 1).

use the w_l adjustments to force strong damping in layers poorly constrained by existing normal mode structure coefficients, regardless of the differences between existing models.

The damped inversion takes the form

$$(\mathbf{M}' + \lambda_1 \mathbf{W}) \cdot \delta\mathbf{v} = \mathbf{\Delta c}' . \tag{10}$$

The damping factor λ_1 is chosen to be large enough to ensure that none of the layer perturbations exceeds the size of the differences between existing models. It is because we employ different weights for each layer and different dampings for each degree that we are able to use the same layers for all inversions. The effective strength of the damping factor is λ_1/N, where N is the number of structure coefficients in an inversion, and is greatest for structural degrees with many layers poorly constrained by the normal mode data. Figure 3b shows $\lambda_1 W_{ll}/N$ for each degree of structure. The odd degrees are damped most severely, and at most degrees the top and bottom of the mantle are damped more strongly than the midmantle.

An output model from an inversion of (10) may be acceptably close to the input model, but it may have moved away from other existing models, increasing the likelihood that it is unacceptably inconsistent with the data used to construct those models. Consistency with all of the various seismic data sets used for modeling is more likely if we explicitly restrict output models to fall "between" existing models. This means that we require our models to differ from any existing model no more than existing models differ from each other. For example, Figure 4 shows that our final model, MM2_L12D8, lies "between" models S12B30 and SKS12WM13 at 1428 km depth, because the amplitudes of the differences between it and each of those models are generally smaller than differences between S16B30 and SKS12WM13.

We ensure that output models lie "between" existing models by inverting for perturbations to sets of input

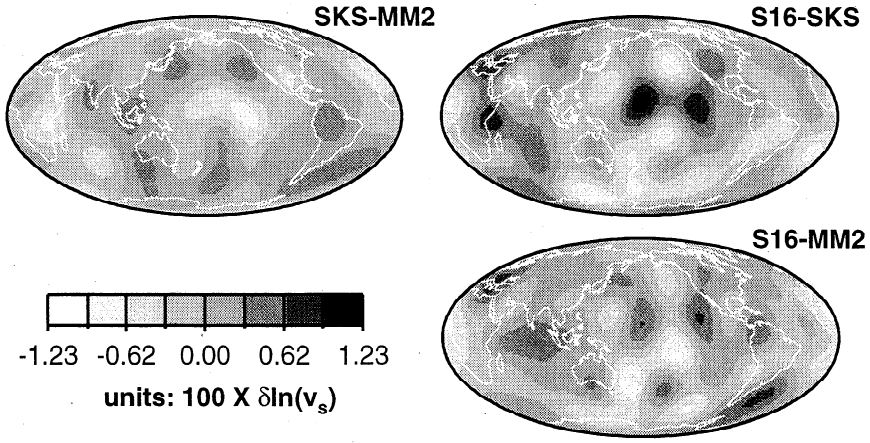

Figure 4. Degree 1-8 differences of three pairs of models in the midmantle (1428 km depth). (top left) Map of the difference between normal mode model MM2_L12D8 (MM2) and SKS12WM13 (SKS). (bottom right) Map of the difference between MM2 and the model S16B30 (S16). (top right) Map of the difference of SKS12WM13 and S16B30. The scale provides the range of MM2_L12D8 at this depth. MM2_L12D8 is generally more similar to the other models than they are to each other.

models that are constrained to produce a single output model. That is, if δv_A and δv_B are perturbations to two 3-D input models v_A and v_B, we require that $v_A+\delta v_A = v_B + \delta v_B$. We can represent such inversions with the equation

$$\begin{pmatrix} \mathbf{M}'+\lambda_1\mathbf{W} & \vdots & \mathbf{0} \\ \cdots & \vdots & \cdots \\ \mathbf{0} & \vdots & \mathbf{M}'+\lambda_1\mathbf{W} \\ \cdots & \vdots & \cdots \\ \lambda_2\mathbf{I} & \vdots & -\lambda_2\mathbf{I} \end{pmatrix} \begin{pmatrix} \delta\mathbf{v}_A \\ \cdots \\ \delta\mathbf{v}_B \end{pmatrix} = \begin{pmatrix} \Delta\mathbf{c}'_A \\ \cdots \\ \Delta\mathbf{c}'_B \\ \cdots \\ \mathbf{v}_B - \mathbf{v}_A \end{pmatrix}, \quad (11)$$

where $\Delta c'_A$ and $\Delta c'_B$ result from the structure coefficients of those input models. Three or more input models could be used in such inversions, but we find it sufficient to employ just two input models at a time. This also allows us to compare the results of using the three possible pairings of the three GBF models (section 3.2.1).

The damping parameter λ_2 is always set large enough to guarantee that the two perturbed models are as close as practical. In practice, output models are usually identical only near the center of each layer because the input models vary differently with radius within each layer. To produce these nearly identical output models, perturbations must achieve some minimum size determined by the difference of the input models. The relative sizes of λ_1 and λ_2 determine how much the perturbations exceed this minimum and how much the output model differs from a simple average of the two input models.

2.4. Overdamping

To make sure that the inversions are not underdamped, we perform a sequence of inversions with λ_1 varying over several orders of magnitude. We characterize these sequences with plots of model amplitude in each layer as a function of the misfit to the structure coefficients achieved by each inversion. Plots for degree 2 inversions are shown in the top three panels of Figure 5.

In every layer there is a damping below which amplitudes are recognizably unstable. Also, as exemplified by the bottom panel of Figure 5, misfit decreases monotonically with the damping parameter. Therefore the best fit that can be achieved without underdamping results from choosing the weakest damping (smallest λ_1) before the onset of instability in any layer. For degree 2, this choice yields $\chi = 2.31$, as indicated in Figure 5. Because the onset of instability is not always obvious, this means of choosing the damping levels is somewhat

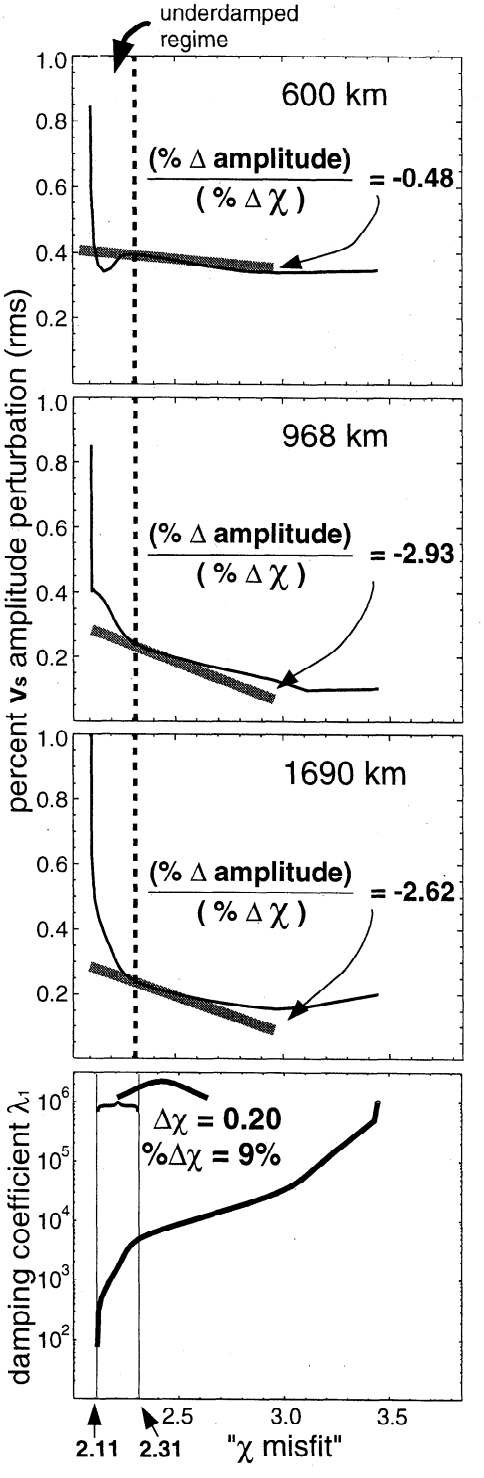

Figure 5. Examples of amplitude stability as a function of misfit and damping. These results are for a suite of inversions to fit degree 2 structure coefficients, which were used to find the damping levels that define model MM2_L12D8. For each inversion the RMS amplitude of aspherical structure in each layer of the resulting v_s model is plotted against the χ misfit (equation (1)). The top three plots show these trends for three different layers. The bottom graph displays damping λ_1 plotted against χ misfit. Vertical lines mark the degree 2 misfit level for model MM2_L12D8 ($\chi = 2.31$) and the asymptotic misfit ($\chi = 2.11$). The percentage slope at $\chi = 2.31$ on the amplitude misfit curves is also indicated. The percentage difference between output model misfit and asymptotic misfit (% $\Delta\chi$) is multiplied by the percentage slope for each layer to find the corresponding percentage amplitude uncertainties of Table 2, subject to a "floor" uncertainty of 20%.

indefinite and leads to some uncertainty in the amplitudes of the final model. We attempt to estimate this uncertainty in section 3.4.1.

2.5. Assembling the Final Model

We have performed sets of inversions at structural degrees 1-6 and 8 using the input model pairs SAW12D and S16B30, S16B30 and SKS12WM13, and SAW12D and SKS12WM13. Our catalogue of structure coefficients does not provide normal mode constraints at degree 7. The crustal model employed is CRUST-5.1 [*Mooney et al.*, 1998]. Model MM2_L12D8 (mode model 2; 12 layers, maximum degree 8) is assembled using whichever of the three output models fits the structure coefficients best at each degree. The model resulting from inputs SKS12WM13 and SAW12D is best at degree 1, and the model with S16B30 and SKS12WM13 as inputs is best at degrees 2, 3, 4, 5, 6, and 8. As noted earlier, our layered parameterization results in two slightly different output models from each inversion. MM2_L12D8 uses the models resulting from perturbations to SKS12WM13, which usually give misfits to the normal mode data a few percent smaller than do the other output models at each degree. Plate 1 shows maps of our model at representative depths. To facilitate comparison with degrees 1-8 maps of other models, maps of MM2_L12D8 include the degree 7 component of SKS12WM13.

3. Assessing the Inversions

To determine whether or not our inversions yield a reliable 3-D v_s model which significantly improves fits to normal mode data, we must establish the following: (1) that fit to the normal mode data is systematically improved by the new model; (2) that our output model is both reasonably independent of our choice of input models and consistent with ("between") those models; (3) that the resolution of these inversions is good enough to yield meaningful images of structure; and (4) that uncertainties are such that our model is robust with respect to inversion damping, effects of unmodeled structure, and errors in the structure coefficients employed.

3.1. Fit to Normal Mode Data

3.1.1. Fit to observed structure coefficients. Model MM2_L12D8 predicts structure coefficients which are significantly closer to the observed coefficients than are the predictions of other models. Figure 6 shows several sets of observed and predicted structure coefficients. Coefficients of a given spherical harmonic component of structure are plotted as functions of the harmonic degree of multiplets along a single fundamental or overtone branch. Multiplets along each of the branches have smoothly varying sensitivities to structure as a function of radius.

As demonstrated by the examples in Figure 6, the predictions of S16B30, SKS12WM13, and SAW12D each fit some observations well and others poorly. The predictions of MM2_L12D8 are systematically closer to the observations than are those of the other models. The improved fit of MM2_L12D8 structure coefficients to the normal mode catalogue is quantified in Table 1. Overall, χ misfit for MM2_L12D8 is $\sim$35% less than that for the predictions of other globally parameterized models. The greatest improvement is at degree 2, which has the greatest number of coefficients constraining the lower mantle. As might be expected, the least improvement is at degrees 1 and 3, which are constrained by only three multiplet pairs and for which inversions are strongly damped. At other degrees, the χ misfit to observed coefficients is improved by 15-40% relative to other models.

There is an unequal distribution of improvement of fit among the various normal mode branches. χ misfit is reduced by 35% to 65% relative to other models for structure coefficients of the ${}_0S$ and ${}_1S$ mode branches. The ${}_0S$ multiplets are primarily sensitive to v_s and ρ variations in the outer lower mantle and transition zone, and to v_p in the upper mantle. The ${}_1S$ modes sample 3-D v_s structure in the lower mantle. In contrast, overall misfits are improved by 15% or less for the ${}_2S$ and ${}_0T$ branches, which are dominantly sensitive to v_s in the upper mantle. Structure coefficients for the lower mantle v_p multiplets of the ${}_4S$ and ${}_5S$ branches are fit no better by MM2_L12D8 than by the predictions of other models.

These observations of residual misfit may be evidence of inadequacies in the parameterization of our present inversions. We expect the ${}_0S$ and ${}_1S$ branches to provide the most important new constraints in the current normal mode catalogue, and our choice of parameterization favors the recovery of the midmantle v_s structures strongly sampled by these branches. It is possible that our radial parameterization of the upper mantle is inadequate to model the v_s structure sampled by ${}_2S$ and ${}_0T$ modes.

Figure 7 demonstrates that misfit to the ${}_0S$, ${}_1S$, ${}_4S$, and ${}_5S$ branches can be appreciably reduced through inversions for models of v_p and ρ which vary independently from v_s. This figure displays examples of the misfit that results from one inversion for v_p structure, and one inversion for v_p and ρ heterogeneity, each with the v_s model fixed at MM2_L12D8. The fits to many of our structure coefficients, like those of the ${}_0S$ branch $\mathrm{Re}(c_6^1)$ coefficients in Figures 6 and 7, are not appreciably improved by breaking the scaling relations. However, misfit to some sets of coefficients [e.g., ${}_4S$-${}_5S$ $\mathrm{Re}(c_2^2)$] can be dramatically reduced by freeing v_p from scaling, while some are improved only through inverting for independent ρ models [e.g., ${}_0S$ $\mathrm{Im}(c_4^3)$], and some [e.g., ${}_1S$ $\mathrm{Re}(c_2^1)$] show improvements attributable to both of these types of heterogeneity. Our inversions for v_p and ρ reduce overall χ misfit by $\sim$ 15%, which is comparable

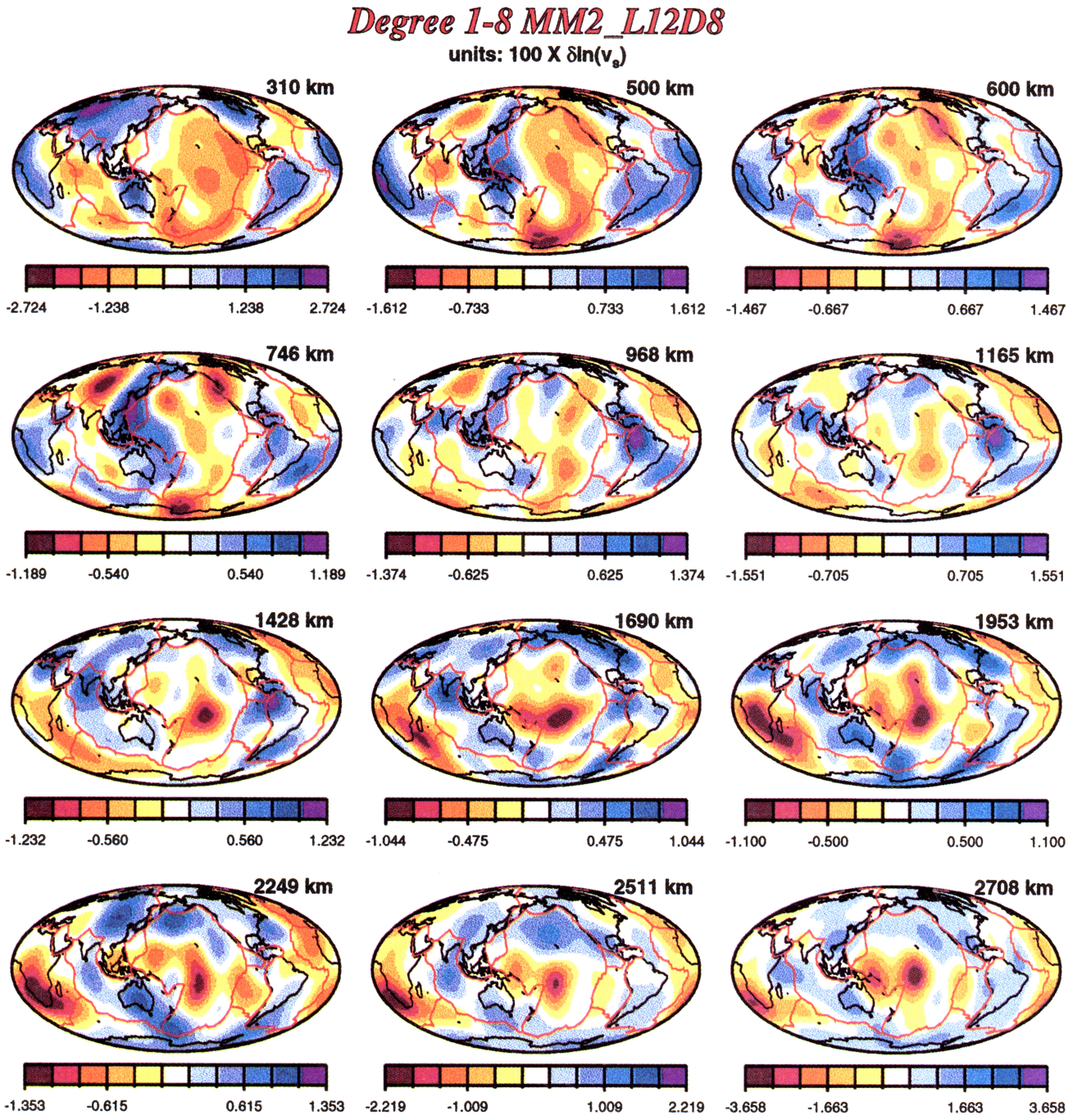

Plate 1. Horizontal slices of normal mode model MM2_L12D8. Slices from the center of each model layer are shown, except that the top layer is not represented and two slices are shown for the upper mantle transition zone. Because MM2_L12D8 does not have a degree 7 component, the degree 7 component of these maps is from model SKS12WM13. Note that a different scale is used for each layer.

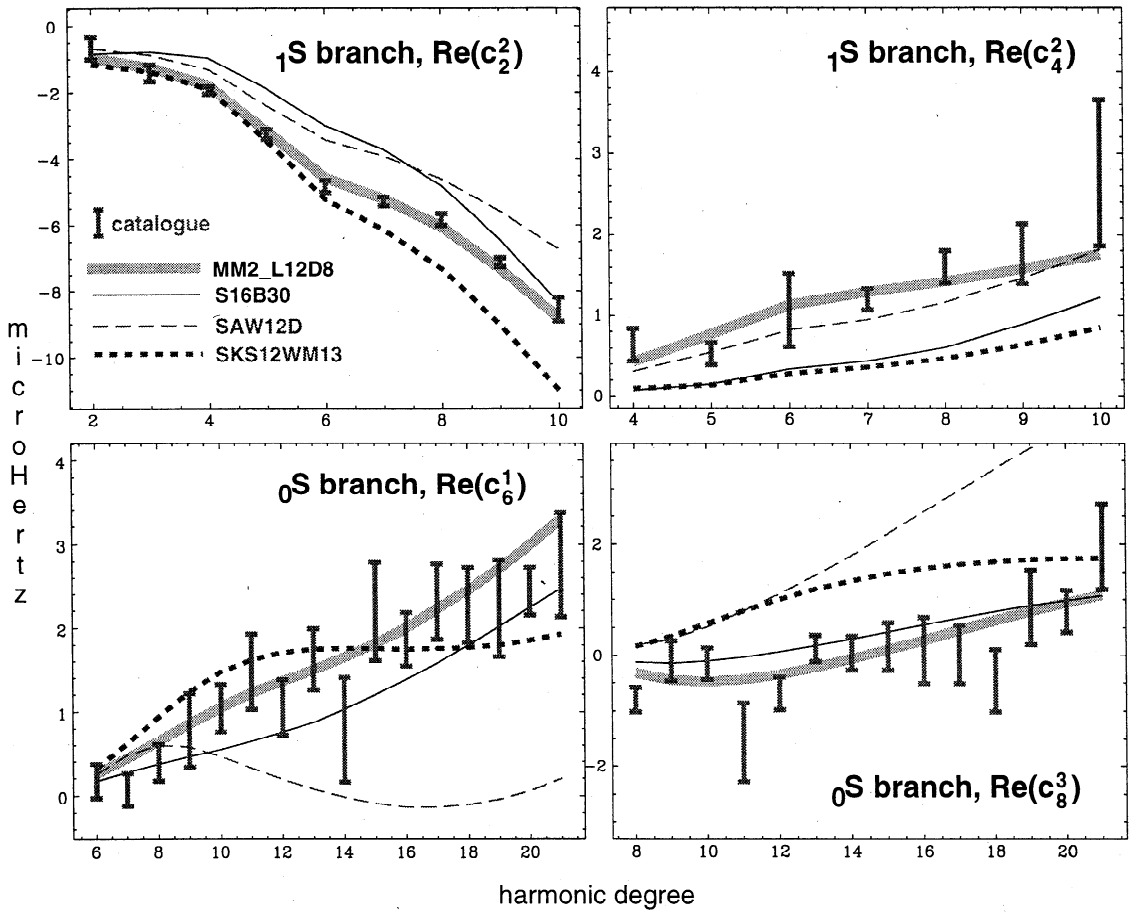

Figure 6. Normal mode structure coefficient measurements together with the predictions from existing models and from MM2_L12D8. Measurements and error bars are from the catalogue of *Resovsky and Ritzwoller* [1998]. Each panel shows structure coefficients at a particular degree and order as a function of multiplet harmonic degree for a single normal mode branch. These examples show variations in the quality of fit of S16B30, SAW12D, and SKS12WM13 to different sets of catalogued coefficients, and the improved fit achieved by model MM2_L12D8.

to the results of *Ishii and Tromp* [1997]. This implies that the normal mode data contain a strong signal from decorrelated v_s, v_p, and ρ structures in the lower mantle and may imply significant chemical heterogeneity. Unfortunately, the structural amplitudes in the resulting models of v_p and ρ are very sensitive to arbitrary choices of damping, and too unreliable for more specific interpretation. This difficulty may be alleviated through the future expansion of the catalogue of normal mode coefficients.

3.1.2. Fit to spectra. Our models have been constrained to fit structure coefficients rather than the actual normal mode spectrum. Therefore it is important to demonstrate that model MM2_L12D8 explains a significant fraction of the signal in this spectrum. In Figure 8 a spectral window incorporating most of our catalogued multiplets displays differences between observed spectra and synthetic spectra generated using either our catalogued estimates of normal mode structure coefficients or coefficients predicted by 3-D Earth models. In the example shown, the MM2_L12D8 synthetic residual is almost as small as that resulting from the estimated coefficients and is at least 30% smaller than those from any of the other models.

Such improvements are typical of the fit of model MM2_L12D8 to high signal-to-noise spectra, although relative misfit varies from multiplet to multiplet and from recording to recording. The general improvement is demonstrated by Figure 9, which shows spectral misfit as a function of signal-to-noise ratio for the data sets used in GSF analyses of two different types of multiplets. The multiplet $_1S_8$ is an isolated overtone multiplet sensitive to v_s variations in the lower mantle, while $_0T_{17}$-$_0S_{16}$ is a pair of surface wave fundamental multiplets coupled by the Coriolis force. In both cases the misfit for MM2_L12D8 synthetics is less than that for the predictions of other models by a fraction that increases with signal-to-noise ratio. This behavior confirms that MM2_L12D8 accounts for a sizable fraction of previously unexplained signal in the free oscillation spectrum.

3.2. Consistency

3.2.1. Consistency of output models. We observe reasonable consistency among the output models that result from different input models. Output models have been constructed from inversions using the

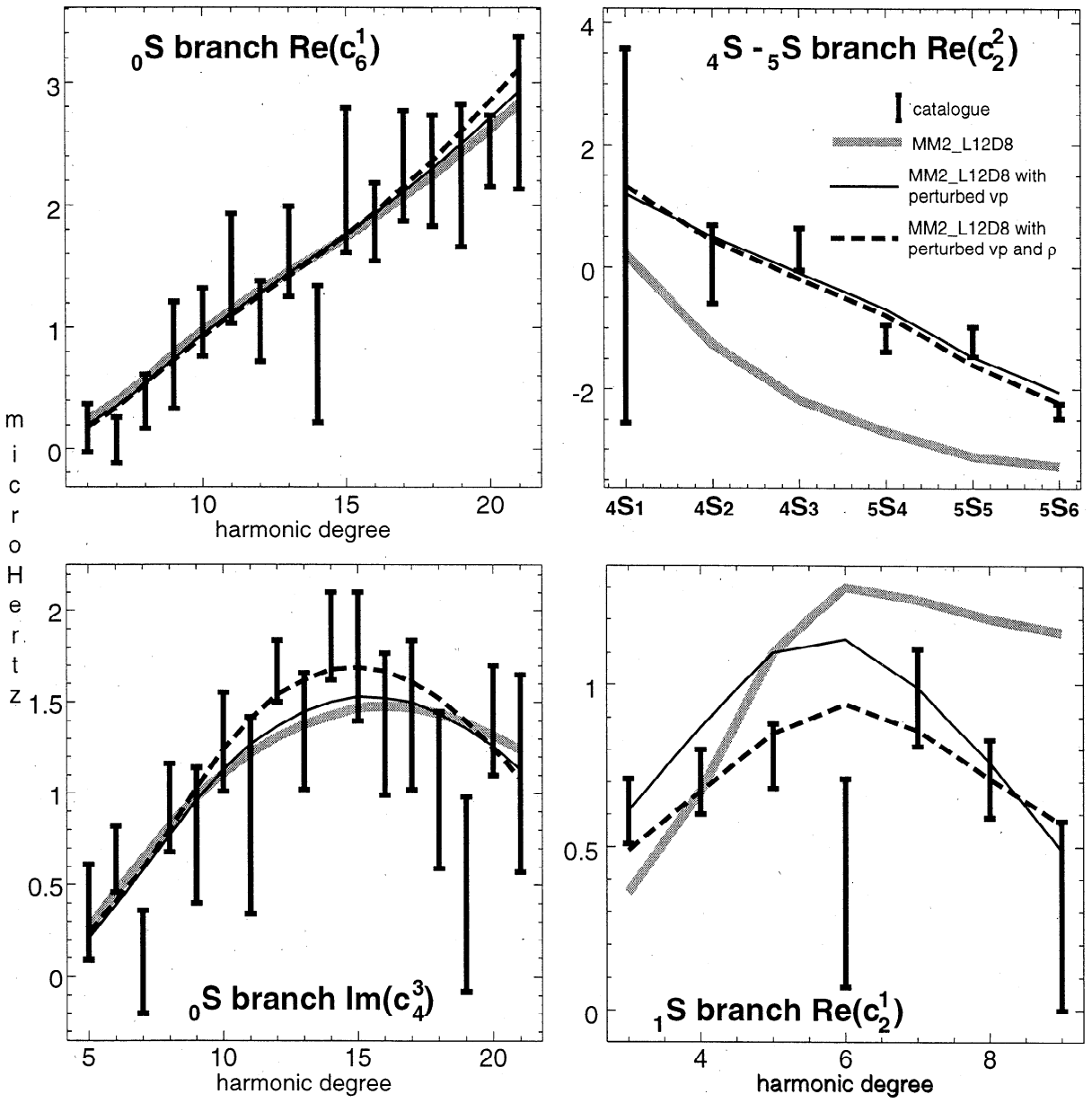

Figure 7. Normal mode structure coefficients predicted by MM2_L12D8 (thick line) and by our models with independent v_s, v_p, and ρ heterogeneities. The thin solid lines result from an inversion for v_p structure, and the thin dashed lines from a simultaneous inversion for v_p and ρ structures. In each case v_s is fixed at MM2_L12D8. Measured values are displayed as error bars.

input model pairs SAW12D and S16B30, S16B30 and SKS12WM13, and SKS12WM13 and SAW12D. These output models yield misfits to the data that differ by less than 1%, even though damping levels are set independently of absolute misfit. The output models are at least 90% correlated throughout the mantle, and differences between them are generally less than half the size of differences between the input models. This is as much consistency as can be expected, given our strategy of keeping the output models relatively close to the selected pair of input models. Figure 10 provides an example of the similarity of output models from inversions using different pairs of starting models.

3.2.2. Consistency with existing models. The model MM2_L12D8 is "between" models SKS12WM13, SAW12D, and S16B30, as defined in section 2.4. Figure 11 displays comparisons of MM2_L12D8 to these input models as functions of radius, in a form similar to Figure 2. Figures 2 and 11 reveal that at each degree and for all depths the new model is more similar to the existing models than they are to each other. This observation holds true for geographic correlations and amplitude ratios as well as for overall model differences. Similarly, the differences between MM2_L12D8 and the Van der Hilst and Grand models (triangles and circles in Figure 11) are consistent with the differences between these models and SKS12WM13 evident in Figure 2.

3.3. Resolution

Two complementary tests of the resolution of model MM2_L12D8 have been performed. We have created artificial models in which realistic long-wavelength 3-D

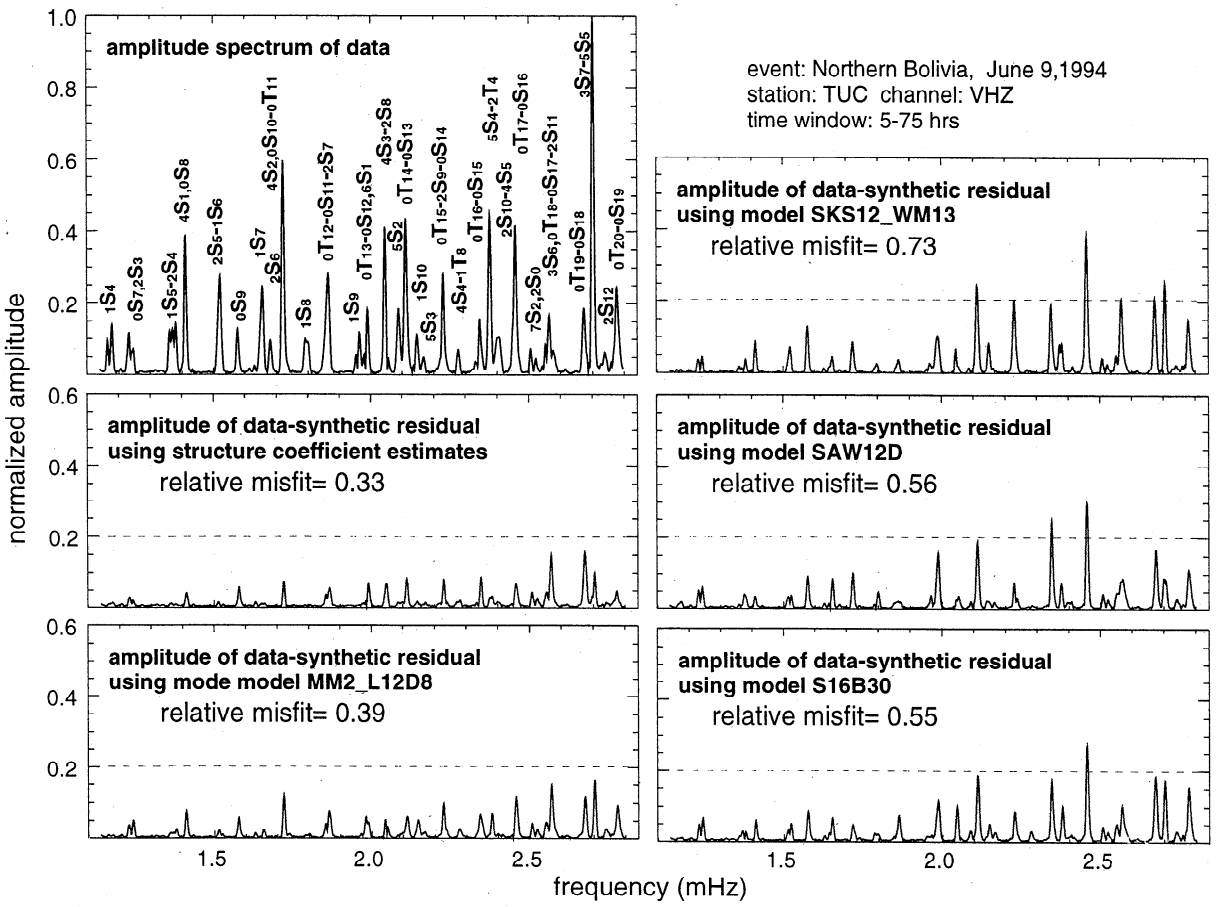

Figure 8. A normal mode spectrum and residuals. A high signal-to-noise spectrum from the deep Bolivian event of 1994 is displayed together with residual spectra which are the amplitude of the difference between the complex data spectrum and various synthetic spectra. The relative misfit given for each residual is its RMS amplitude divided by the RMS amplitude of the data spectrum. The horizontal lines at the 0.20 amplitude level provide a reference for visual comparisons of the spectra.

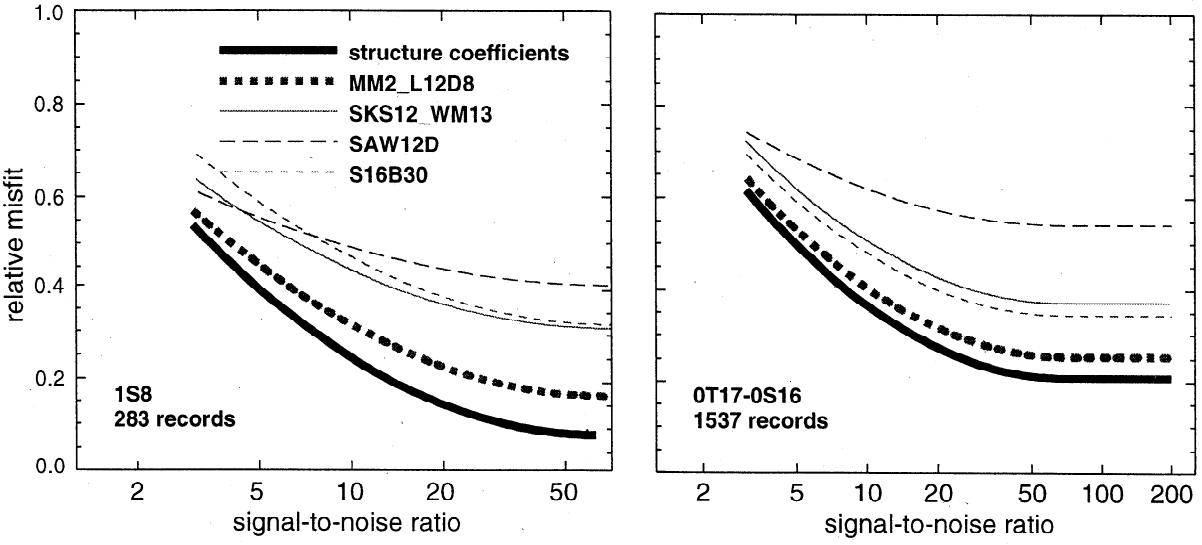

Figure 9. Relative misfit (see Figure 8 caption) as a function of signal-to-noise ratio for narrow spectral windows about individual multiplet groups. The curves shown are parameterized fits to the observed distribution of misfits. *Resovsky and Ritzwoller* [1998] provides further discussion of these fits. Multiplet ${}_1S_8$ is isolated and is primarily sensitive to v_s in the lower mantle. The Coriolis-coupled pair ${}_0T_{17}$-${}_0S_{16}$ are long-period surface wave multiplets sensitive to the upper mantle. Misfits for both groups achieve high signal-to-noise asymptotes above which misfit is dominated by errors in the models and synthetics rather than by noise.

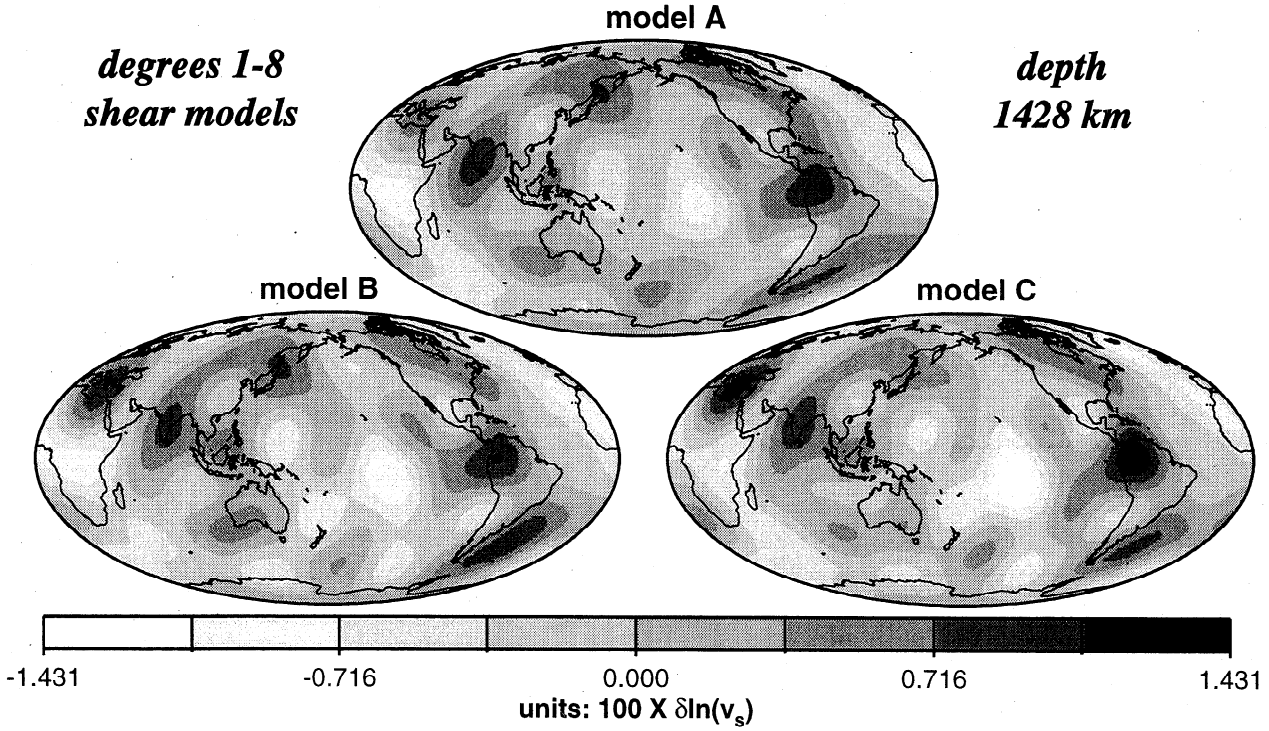

Figure 10. Results of inversions using different input models. These inversions fit normal mode data using three different pairs of starting models, and these maps typify the similarity of the output models. Model A employs SKS12WM13 and S16B30 as inputs, model B employs S16B30 and SAW12D, and model C employs SAW12D and SKS12WM13.

structure either is confined to single layers or is absent (null) only in three adjacent layers. These test models are used to generate sets of noise-free synthetic structure coefficients, which are inverted using the same scheme and damping used in the construction of model MM2_L12D8. Inversions of synthetic coefficients from the single-layer models show the leakage of estimated structure out of each layer, while inversions of null-layer synthetic coefficients demonstrate the leakage into each layer from above or below.

The top panel of Figure 12 shows a single-layer resolution test model for a midmantle layer. This model was created using the degree 1-8 components of the positive velocity anomalies of the Van der Hilst model at the selected depth. The bottom panels of Figure 12 display maps of the output model from the corresponding inversion test. Each map shows the center of a different layer. The map corresponding to the input layer is better than 95% correlated with the input model at each structural degree. Amplitudes in this layer are within 10% of the input amplitudes, except at degrees 1 and 3 (15% and 25% differences, respectively) which are sampled by coefficients of only three multiplet pairs. The amplitude of the output model in all layers outside the input layer is less than 1/3 of the input model. Outside the depth range shown, amplitudes are less than 1/6 of the input amplitude.

The results of two null-layer resolution tests are shown in Figure 13. The null layers of the input models are the center three layers in each column. The use of input models with three-layer null blocks allows us to identify separately leakage into midmantle layers from above and from below. Throughout the transition zone and midmantle, radial leakage into the gaps has amplitudes less than 20% of the corresponding amplitudes of model MM2_L12D8 and is poorly correlated with the model.

We conclude that our inversions should produce only weak leakage of structure out of or into any midmantle layer. The existing structure coefficient catalogue and the inversion strategy we employ are adequate to retrieve probable mantle structures between 200 and 2700 km depth with a radial resolution roughly equivalent to the selected layer widths, provided that other forms of modeling uncertainty are not too strong.

3.4. Model Uncertainty

3.4.1. Uncertainty from inversion damping. We observe that at some depths and for some degrees the amplitudes of our output models are strongly dependent upon our choices of damping and radial weighting. This implies that there is an appreciable range among the amplitudes of plausible v_s models that fit the normal mode structure coefficients.

To assign amplitude uncertainties, we need to estimate the ranges of amplitudes among v_s models that fit structure coefficients reasonably well. By "reasonably well" we mean nearly as well as or better than

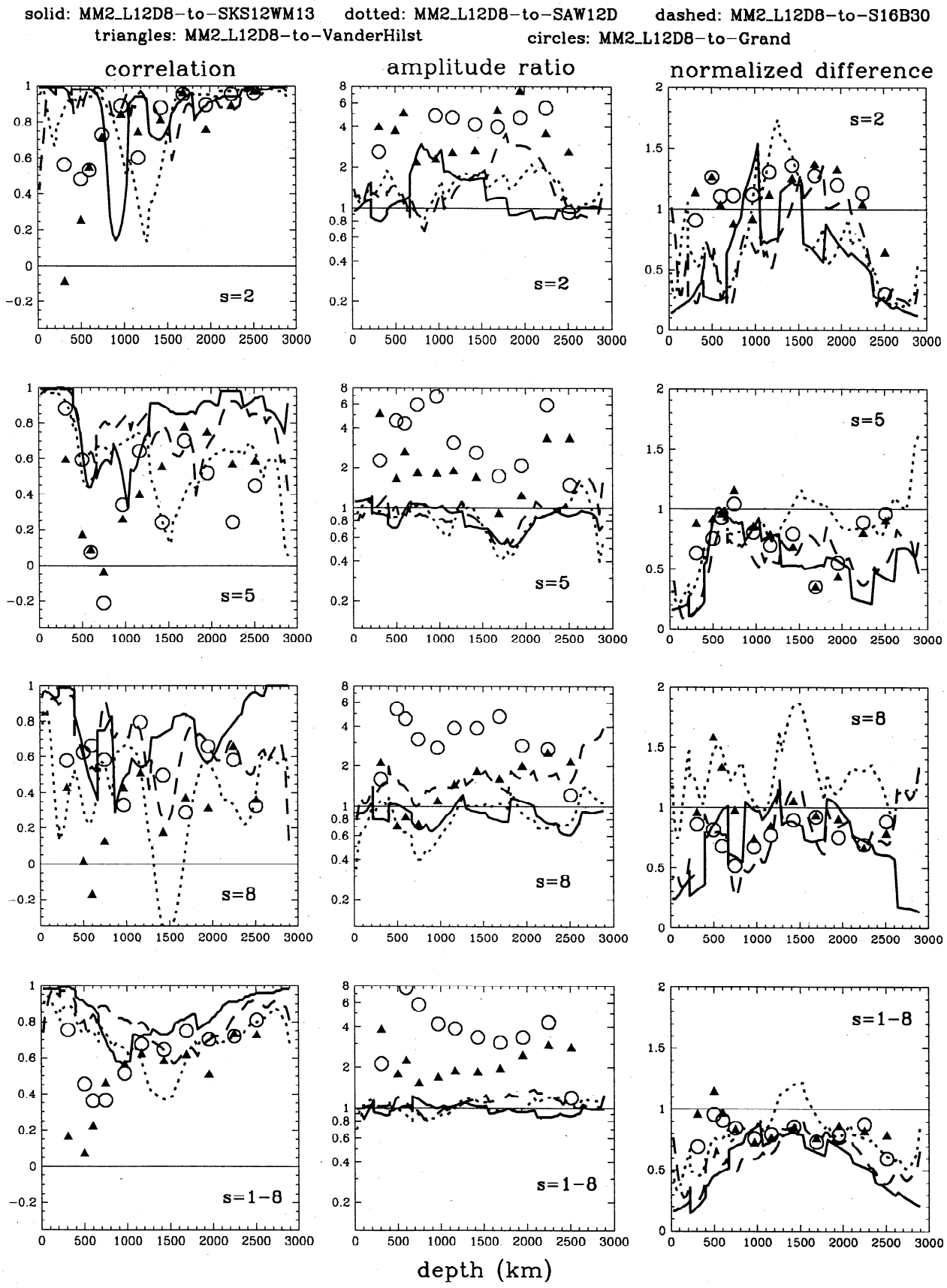

Figure 11. Radial comparisons of MM2_L12D8 to other mantle models, in the same format as that of Figure 2. All model differences at any depth are normalized by the average of the RMS amplitudes of models SKS12WM13, S16B30, and SAW12D at that depth. For the degree 1-8 comparisons, the (unconstrained) degree 7 part of model MM2_L12D8 is set equal to the degree 7 component of that model to which it is compared.

MM2_L12D8. Models which fit the data nearly as well as MM2_L12D8 are readily explored using suites of overdamped inversions with a variety of starting models and layerizations. Our experiments with such models yield amplitude variations at degrees 2, 4, 5, 6, and 8 that are consistently 20% or smaller among models that fit the normal mode data no more than 10% worse than MM2_L12D8. Thus we set the lower limit of amplitude uncertainty to 20% for any depth at these degrees. For degrees 1 and 3, which are constrained by only three multiplet pairs and have few independent spherical harmonic components of structure, observed variability of RMS amplitudes is greater. Minimal uncertainty is 50% for degree 1 and 33% for degree 3.

Amplitude uncertainties need to be still larger at some degrees and for some layers. In these cases, amplitude instability has no clear onset as a function of damping. A conservative choice of damping in such layers introduces the possibility of a stable model with different amplitudes that fits the normal mode data better than MM2_L12D8. There is no rigorous means of accounting for this uncertainty, but we can make the following observations: (1) that clear amplitude instability is associated with large slopes in amplitude versus misfit plots (Figure 5); (2) that the ambiguous onset of amplitude instability can therefore be associated with larger than usual slopes at the points corresponding to selected damping levels; (3) that plots of overall (λ_1) damping versus misfit generally exhibit a vertical asymptote at low damping, as in the bottom panel of Figure 5; (4) that adjusting layer damping levels to the point where all layer amplitudes are clearly unstable generally yields misfits near the asymptotes for overall damping.

These observations motivate a two-step procedure for assigning amplitude uncertainty above the minimal values for each degree. This procedure is demonstrated in Figure 5. We first estimate a potential percentage improvement to misfit (% $\Delta\chi$) using the difference between the asymptotic misfit and the misfit produced at the damping level selected for our inversions. We then find each layer's percentage slope, (%Δamplitude)/(%$\Delta\chi$), at the selected damping level and multiply this by %$\Delta\chi$ to obtain amplitude uncertainty. The final amplitude uncertainties assigned to each layer for each degree are shown in Table 2. In most cases, we have found that amplitude uncertainties for structures in model MM2_L12D8 are less than $\sim$ 35%. The 100% uncertainties assigned for degree 1 amplitudes near 1000 and 2000 km depths indicate that

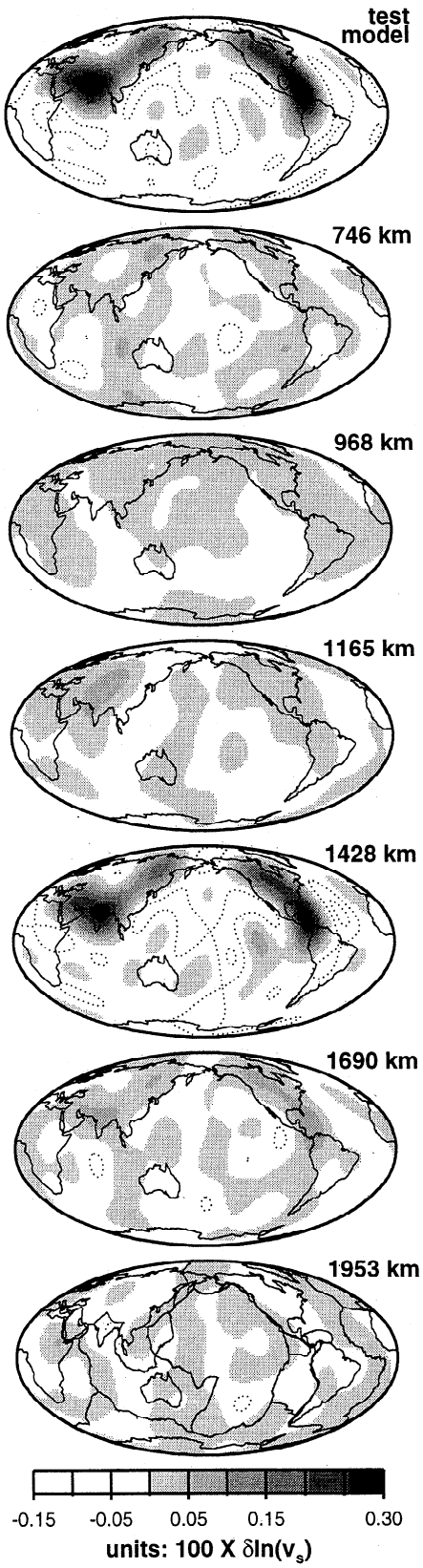

Figure 12. Maps of the input and output models from a single-layer test of resolution. At top is the input model, which is constant in a single layer centered on 1428 km depth and null in all other layers. This model is the degrees 1-8 component of the positive velocity portion of the Van der Hilst model at 1500 km depth (negative velocity sidelobes result from the low-degree truncation). Below are maps of the degrees 1-8 components of the model produced by inverting the synthetic structure coefficients from the input model. The layers shown are the only ones for which significant structure is observed in the output model. Dotted lines indicate the -0.05% and -0.10% $d\ln v_s$ contours.

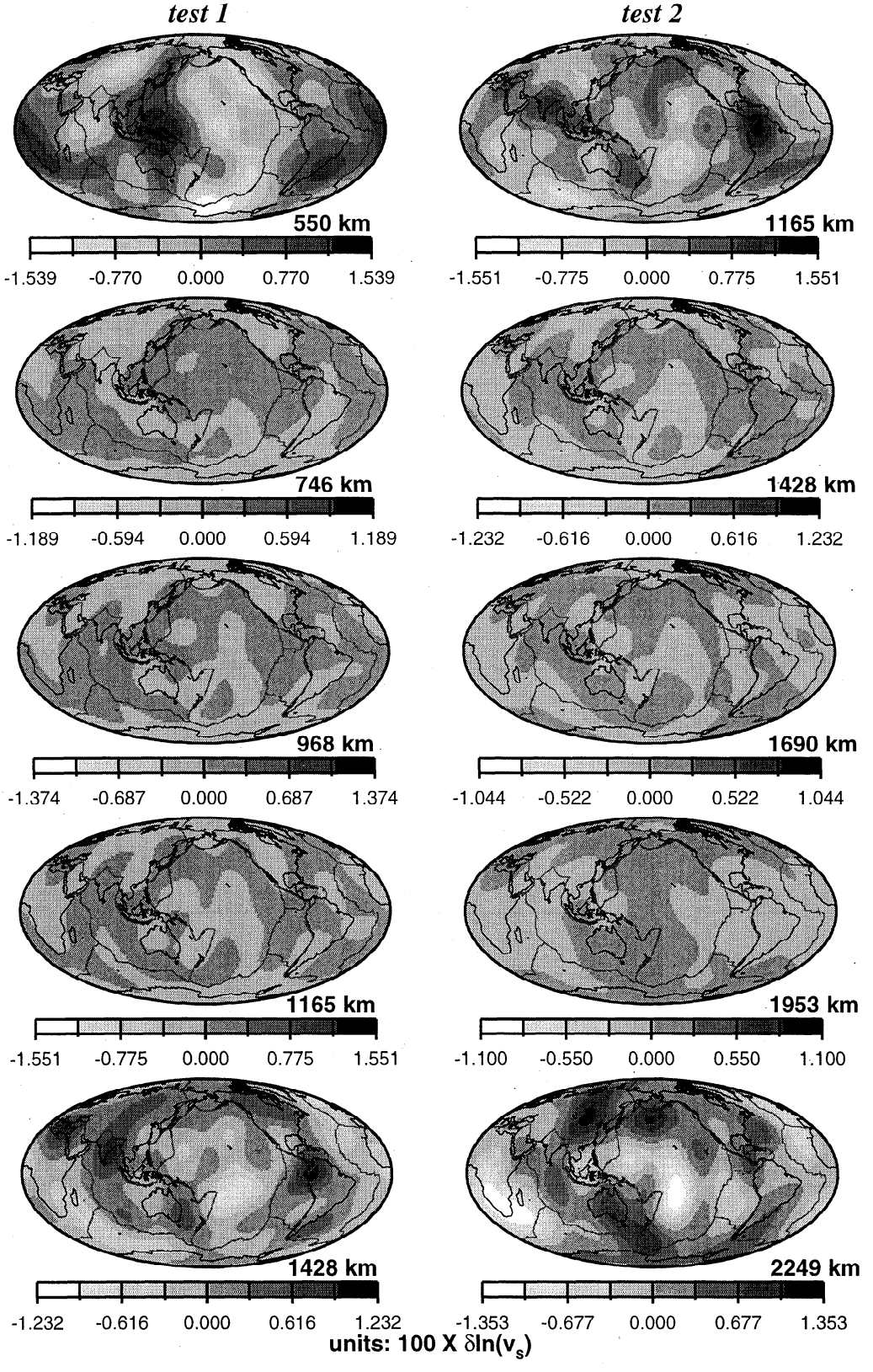

Figure 13. Maps of the output models from two synthetic inversions with "null" layer inputs. The middle three maps of each column are the null layers. Contour levels are those for the corresponding layers of model MM2_L12D8 (see Plate 1).

Table 2. Amplitude Uncertainty Estimates

Depth,	Percent Amplitude Uncertainty						
km	$s=1$	$s=2$	$s=3$	$s=4$	$s=5$	$s=6$	$s=8$
2708	50	20	33	20	23	20	50
2511	82	20	33	20	20	20	20
2249	39	20	33	20	20	20	20
1953	100	20	33	21	43	20	24
1690	50	24	33	23	70	34	20
1428	50	24	33	35	20	60	23
1165	51	20	33	22	25	34	20
968	100	26	33	20	34	20	20
746	57	20	41	20	36	40	20
600	50	20	33	20	51	20	20
500	50	20	33	25	20	20	20
310	50	20	33	20	20	20	20
103	50	20	50	20	20	20	20

we have no confidence in our ability to resolve degree 1 structure at those depths.

We have performed similar analyses of the uncertainty in model geometry associated with our choice of damping parameters and find that the models which fit the data reasonably well at each degree are correlated at better than 99% confidence at all depths. The only exception to this rule is for degree 1 models at the unresolvable depths noted above.

3.4.2. Uncertainty in v_s from v_p and ρ. We have also estimated the amplitude uncertainty for normal mode models of v_p and ρ, as well uncertainty in our v_s model that is associated with unspecified v_p and ρ heterogeneity. We find that moderate changes in inversion damping produce a relatively wide range of v_p and ρ models which all yield 15–20% improvements in the fit to the normal mode structure coefficients. Amplitudes among such models differ by more than 100% throughout much of the mantle. For this reason, we do not believe that robust models of v_p and ρ can be obtained through inversions of the existing normal mode data, unless, perhaps, geodetic and/or geodynamic constraints are applied.

Nonetheless, this suite of independent v_p and ρ models is useful for estimating the effects of uncertainties in such structures on our inversions for v_s models. To do this, the new v_p and ρ models are used to replace the scaled v_p and ρ in inversion starting models, and we perform new inversions for independent v_s structure. The resulting v_s models are compared to MM2_L12D8. The largest amplitude perturbations observed in these experiments are shown in Figure 14a. Amplitude perturbations relative to MM2_L12D8 are smaller than the uncertainties from indefinite damping reported in Table 2, and correlations with MM2_L12D8 are above the 99.9% confidence level, except for the unresolved depths of degree 1. We have also investigated the consequences

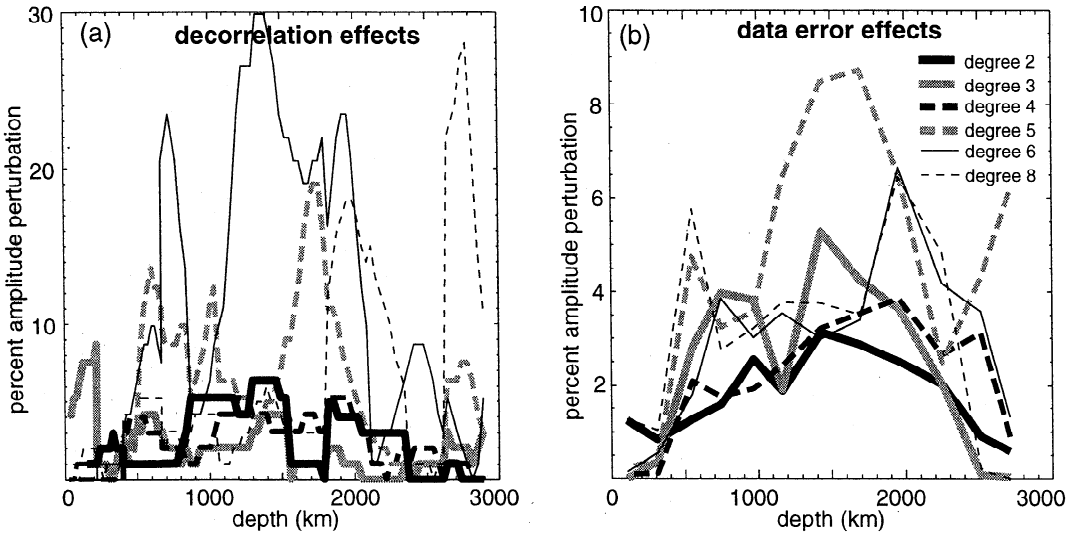

Figure 14. Estimated effects on v_s structure resulting from decorrelated v_p and ρ and from data errors. (a) The v_s amplitude perturbations relative to MM2_L12D8 for models due to independent v_p and ρ input models. We perform new inversions for v_s structure in which the input models of v_p and ρ come from normal mode inversions with the v_s model fixed at MM2_L12D8, rather than from scaling relations. The result of each new inversion is compared with MM2_L12D8. The curves for each degree of structure represent the largest relative amplitude difference observed at each depth. (b) Mean results of amplitude comparisons with MM2_L12D8 for a Monte Carlo test of sensitivity to data errors. Suites of output models are generated from inversions of Monte Carlo perturbations to the normal mode data. Fifty sets of perturbed data were used for each degree, and the perturbations of each structure coefficient conform to normal distributions about the catalogued value matching the catalogued standard deviations.

of maintaining the scaling between v_s, v_p, and ρ, while allowing the scaling factors to vary. These effects are no larger than those above, even when α in the uppermost and lowermost mantle is set to values that may result from partial melt ($\alpha \cong 0.35$). Thus we expect that the effects of plausible models of v_p and ρ on our v_s inversions to be smaller than the reported uncertainties associated with damping.

Finally, the effects of potential errors in the crustal model, the mislocation of discontinuities in the upper mantle, and anisotropy near the top and bottom of the mantle all have relatively small impacts on our v_s models because of the strong damping we employ in the uppermost and lowermost mantle (section 2.3 and Figure 3).

3.4.3. Uncertainty from measurement error. To estimate the uncertainties in our inversions associated with the reported measurement errors for normal mode structure coefficients, we have performed a Monte Carlo experiment with the data. Each observed structure coefficient is perturbed by a random deviate which conforms to a normal distribution about its measured value with a standard deviation equal to the uncertainty reported by *Resovsky and Ritzwoller* [1998]. These perturbed coefficients are inverted for a new v_s model. This procedure is repeated several dozen times, and each resulting model is compared to MM2_L12D8. Figure 14b shows the mean amplitude perturbations from MM2_L12D8 for this set of models, at each degree and depth. Once again, correlations with MM2_L12D8 are above the 99.9% confidence level, except for the unresolved depths of degree 1, and amplitude perturbations are generally less than half the size of the uncertainties assigned in Table 2. This table is therefore adequate to express the amplitude uncertainty in our inversions, and we can assume that the range of model geometries implied by normal modes is within the 99% confidence level of model MM2_L12D8.

4. Characteristics of MM2_L12D8

4.1. Amplitude

We can use the amplitude uncertainty estimates of Table 2 to compare the amplitude spectrum of model MM2_L12D8 to that of other models, independent of model geometry. Uncertainties in amplitudes are usually less than $\sim$35%, except for degree 1, which does not contribute much to the overall amplitude of the model. Because the RMS amplitudes of degree 1-8 structure in MM2_L12D8 are generally within 35% of the amplitudes of the GBF models SKS12WM13, SAW12D, and S16B30, but usually more than twice those of the LBF models of Van der Hilst and Grand (see Figure 11), MM2_L12D8 clearly favors the amplitudes of existing models that use GBFs. More recent LBF models, such as the v_s and v_p models of *Vasco and Johnson* [1998], are reducing this amplitude discrepancy, and yield fits to structure coefficients comparable to fits from GBF models.

In Figure 15 we compare the amplitude spectrum of MM2_L12D8 with those of other GBF models. The figure shows the RMS amplitudes of aspherical v_s structure at degrees 1-8 for eight different depths in the transition zone and lower mantle. Values for MM2_L12D8 are plotted with error bars derived from Table 2. For degrees 3-8 the normal mode inversions yield amplitudes that are generally consistent with the other models. At these degrees amplitudes usually decay smoothly with decreasing wavelength and are roughly constant through all but the uppermost and lowermost mantle. MM2_L12D8 has dominant degree 2 structure throughout the depth range shown, although the amplitude of degree 2 relative to the amplitudes at other degrees is smallest near the center of the mantle. Our resolution tests (section 3.3) demonstrate that this characteristic is not attributable to radial leakage of higher amplitude structures in the upper mantle and D'' into the midmantle. Predominant degree 2 structure in the upper mantle and lowermost mantle is quite familiar [e.g., *Su and Dziewonski*, 1991], and we match the degree 2 amplitude of SKS12WM13 in the transition zone and below 1800 km depth and that of S12B30 and SAW12D between 670 and 1200 km depth, but the persistent dominance of degree 2 structure in the midmantle is unique to our model.

4.2. Structure

Relative to SKS12WM13, SAW12D, S16B30, the models of Van der Hilst and Grand, and other recently published models, the structural features of MM2_L12D8 fall into four categories: (1) features present in all other global models, (2) features present in only a subset of the other models, (3) features which appear to be a compromise of structures which vary from model to model, and (4) features which are unique to our model. We will endeavor to point out examples of each type of feature, but readers who wish to make more detailed comparisons are encouraged to retrieve and examine the model maps that we have made available on our web site.

Category 1 features, those which our model shares with all other models, include the long-wavelength components of all the continental shields in the uppermost mantle. Category 2 includes low-velocity features in the transition zone. The low velocities under the Pacific in MM2_L12D8 match those of SKS12WM13 and S16B30, but those of SAW12D look significantly different. MM2_L12D8 also favors a high-velocity anomaly near 1000 km depth below northern South America in SAW12D and low-velocity anomalies under Antarctica at 670-1000 km depths in S16B30.

Category 3 is best represented by the patterns of high-velocity anomalies in the 950-1500 km depth range, some of which are evident in Figure 1. The geometry and relative amplitudes of both low- and high-

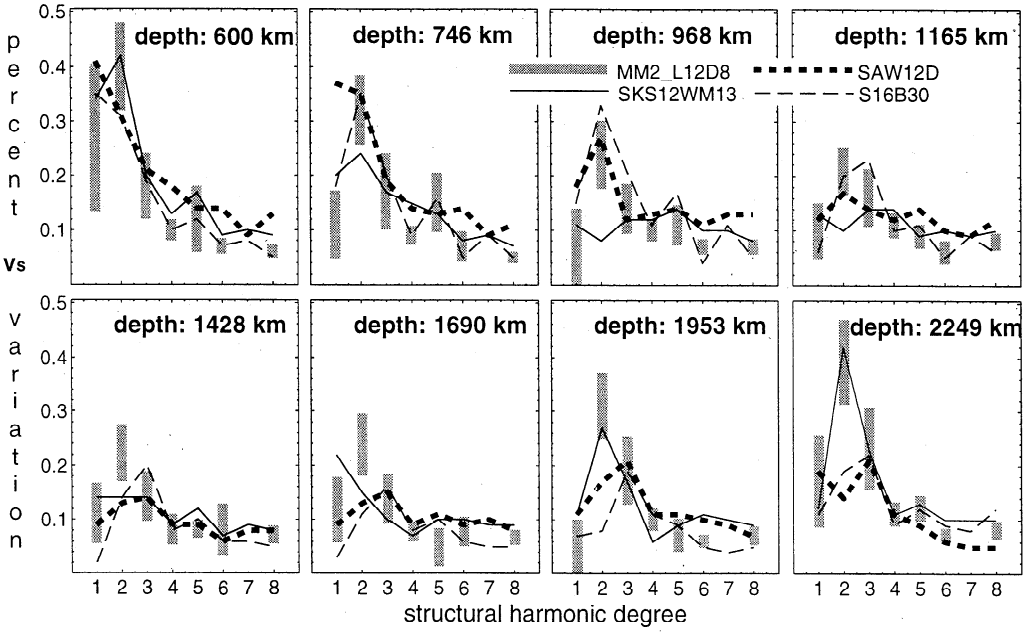

Figure 15. Amplitudes of aspherical structure in 3-D mantle models. At each depth, these plots show the RMS amplitude of lateral heterogeneity at spherical harmonic degrees 1-8. The values for model MM2_L12D8 are shown as ranges calculated using Table 2. Degree 7 does not exist for model MM2_L12D8.

velocity structures at 1428 km depth vary considerably from model to model, but MM2_L12D8 resembles them all about equally. Under northern South America, MM2_L12D8 has a strong high-velocity anomaly throughout the 950-1500 km depth range. Its amplitude, relative to other features, is most similar to the corresponding anomaly in the Grand and Van der Hilst models, or to SAW12D at slightly shallower depths. However, its shape in MM2_L12D8 is rounded, as in the GBF models, rather than elongated, as in the LBF models.

Category 4 features, those unique to MM2_L12D8, include the high-velocity anomaly to the south and east of South America. This structure appears to extend from the transition zone downward to at least 2000 km depth. The category 3 high-velocity anomaly under northern South America may also be classified as category 4, because its amplitude in MM2_L12D8 is significantly greater than in any other model.

Taken together, these features produce a model of the transition zone and lower mantle with new images of both "slab-like" and "plume-like" structures in the midmantle. In the probable locations of the subducted Tethys and Farallon slabs [*Jordan and Lynn*, 1974; *Van der Hilst et al.*, 1997; *Grand et al.*, 1997], we find strong high-velocity anomalies. The strength of these anomalies relative to other midmantle features is reminiscent of the LBF models, but they manifest little "slab-like" elongation in our model. There are two main "plume-like" low-velocity structures which extend upward from the core-mantle boundary (CMB) beneath Africa and the Pacific. MM2_L12D8, more clearly than other models, shows both of these features continuing through the midmantle and possibly feeding into the very strong low velocities beneath the southern Pacific triple junction in the uppermost lower mantle and transition zone.

5. Conclusions

We have constructed the degree 8 mantle v_s model MM2_L12D8 with inversions of normal mode structure coefficients that complement the structural sensitivities of surface wave and body wave data used to constrain most seismic models. These inversions demonstrate that robust and plausible perturbations to existing mantle models can greatly improve the fit to normal mode data and can provide refined images of structures in the midmantle (900-1800 km depths).

The most notable results of this investigation are as follows. (1) Though MM2_L12D8 has been constrained to lie "between" existing models (our proxy for maintaining consistency with other seismic data) it reduces χ misfit (equation (1)) to structure coefficients by at least 35% relative to those models. (2) MM2_L12D8 is robust relative to choices of damping, unmodeled structure, model parameterization, and data errors, with amplitude uncertainties generally estimated to be less than $\sim 35\,\%$. (3) Indefinite choices of damping are the dominant source of uncertainty in inversions of normal mode structure coefficients. (4) In inversions for independent models of v_s, v_p, and ρ, uncertainty due to damping is large enough that the resulting v_p and ρ models are unreliable, but the normal mode data clearly exhibit a significant signal from decorrelated v_s, v_p, and ρ structures

in the lower mantle. (5) MM2_L12D8 is most different from existing models in the midmantle, where significant inconsistencies among those models are evidence of relatively weak structural constraints from other seismic data.

In the midmantle, MM2_L12D8 exhibits strong high-velocity features reminiscent of structures most evident in models which use local basis functions (LBFs) but without the "slab-like" elongation seen in those models. Low-velocity "plumes" in MM2_L12D8 follow paths up from the CMB similar to those of models that use global basis functions (GBFs) but are more clearly continuous through the midmantle than previous models have suggested. MM2_L12D8 clearly favors the amplitudes of long-wavelength structure seen in GBF models, as opposed to the much smaller amplitudes of the LBF models. Both "slabs" and "plumes" in the midmantle of MM2_L12D8 are dominated by a degree 2 component of structure which is stronger and more consistent as a function of depth in our model than in others. Because MM2_L12D8 exhibits this consistency of amplitude spectra with depth, and because it has features which resemble downgoing "slabs" and upgoing "plumes" passing through the midmantle, our normal mode inversions suggest that the midmantle participates in a very long wavelength convective system incorporating at least the whole of the lower mantle.

These results provide strong motivation for future exploitation of the unique sensitivity of normal mode data to mantle structures. Among the most compelling avenues for future research are more thorough investigations of misfits and uncertainties in simultaneous normal mode inversions for independent models of v_s, v_p, and ρ; the extension of the normal mode catalogue to improve the resolution and reliability of normal mode models; and the union of available seismic, geodetic, and geodynamic constraints with normal mode data in new inversions for mantle structure. To encourage the exploration of these issues we will continue to make our normal mode catalogue and mantle v_s models available at the web site physgeophys.colorado.edu/geophysics/nm.dir.

Acknowledgments. We greatly appreciate the instructive questions of Ruedi Widmer-Schnidrig, an anonymous reviewer, and our associate editor. The funding for this research was provided by NSF grant EAR-97-06188. We wish to thank Xian-Feng Liu, Barbara Romanowicz, Guy Masters, Rob Van der Hilst, and Steven Grand for making their mantle models available.

References

Anderson, O. L., E. Schreiber, R. C. Lieberman, and M. Soga, Some elastic constant data on minerals relevant to geophysics, *Rev. Geophys., 6,* 491-524, 1968.

Bijwaard, H., W. Spakman, and E. R. Engdahl, Closing the gap between regional and global travel time tomography, *J. Geophys. Res.,* in press, 1998.

Dziewonski, A. M., and D. L. Anderson, Preliminary reference Earth model, *Phys. Earth Planet. Inter., 25,* 297-356, 1981.

Giardini, D., X.-D. Li, and J. H. Woodhouse, Three dimensional structure of the Earth from splitting in free oscillation spectra, *Nature, 325,* 405-411, 1987.

Giardini, D., X.-D. Li, and J. H. Woodhouse, The splitting functions of long period normal modes of the Earth, *J. Geophys. Res., 93,* 13,716-13,742, 1988.

Grand, S. P., R. D. van der Hilst, and S. Widiyantoro, Global seismic tomography: A snapshot of convection in the Earth, *GSA Today, 7*(4), 1-7, 1997.

He, X., and J. Tromp, Normal-mode constraints on the structure of the Earth, *J. Geophys. Res., 101,* 20,053-20,082, 1996.

Ishii, M., and J. Tromp, Three-dimensional modeling of mantle heterogeneity using normal-mode splitting function coefficients (abstract), *Eos Trans. AGU, 78*(46), Fall Meet. Suppl., F460, 1997.

Jordan, T. H. and W. S. Lynn, A velocity anomaly in the lower mantle, *J. Geophys. Res., 79,* 2679-2685, 1974.

Karato, S., Importance of anelasticity in the interpretation of seismic tomography, *Geophys. Res. Lett., 20,* 1623-1626, 1993.

Li, X.-D., and B. Romanowicz, Global mantle shear-velocity model developed using nonlinear asymptotic coupling theory, *J. Geophys. Res., 101,* 22,245-22,272, 1996.

Li, X.-D., D. Giardini, and J. H. Woodhouse, Large-scale three-dimensional even-degree structure of the Earth from splitting of long-period normal modes, *J. Geophys. Res., 96,* 551-557, 1991.

Liu, X.-F., The three-dimensional shear-wave velocity structure of the Earth's lowermost mantle, Ph.D. thesis, Harvard Univ., Cambridge, Mass., 1997.

Liu, X.-F., and A. M. Dziewonski, Improved resolution of the lower-most mantle shear wave velocity structure obtained usng SKS-S data (abstract), *Eos Trans. AGU, 75*(16), Spring Meet. Suppl., S232, 1994.

Masters, G., H. Bolton, and P. Shearer, Large-scale 3-dimensional structure of the mantle (abstract), *Eos Trans. AGU, 73*(43), Fall Meet. Suppl., F201, 1992.

Masters, G., S. Johnson, G. Laske, and H. Bolton, A shear-velocity model of the mantle, *Philos. Trans. R. Soc. London, Ser. A, 354,* 1385-1411, 1996.

Mooney, W. D., G. Laske, and G. Masters, CRUST 5.1: A global crustal model at 5° by 5°, *J. Geophys. Res., 103,* 727-748, 1998.

Resovsky, J. S., and M. H. Ritzwoller, Constraining odd-degree mantle structure with normal modes, *Geophys. Res. Lett., 22,* 2301-2304, 1995.

Resovsky, J. S., and M. H. Ritzwoller, New and refined constraints on three-dimensional Earth structure from normal modes below 3 mHz, *J. Geophys. Res., 103,* 783-810, 1998.

Ritzwoller, M. H., and E. M. Lavely, Three-dimensional seismic models of the Earth's mantle, *Rev. Geophys., 33,* 1-66, 1995.

Ritzwoller, M. H., and J. S. Resovsky, The feasibility of normal mode constraints on higher degree structures, *Geophys. Res. Lett., 22,* 2305-2308, 1995.

Ritzwoller, M. H., G. Masters, and F. Gilbert, Constraining aspherical structure with low harmonic degree interaction coefficients: Application to uncoupled multiplets, *J. Geophys. Res., 93,* 6269-6396, 1988.

Robertson, G. H., and J. H. Woodhouse, Ratio of relative S to P velocity heterogeneity in the lower mantle, *J. Geophys. Res., 101,* 20,041-20,052, 1996.

Su, W.-J., and A. M. Dziewonski, Predominance of long-wavelength heterogeneity in the mantle, *Nature, 352,* 121-126, 1991.

Su, W.-J., and A. M. Dziewonski, Degree 12 model of shear velocity heterogeneity in the mantle, *J. Geophys. Res., 99,* 6945-6980, 1994.

Thoraval, C., and M. A. Richards, The geoid constraint in global geodynamics: Viscosity structure, mantle heterogeneity models and boundary conditions, *Geophys. J. Int., 131,* 1-8, 1997.

Tromp, J., and E. Zanzerkia, Toroidal splitting observations from the great 1994 Bolivia and Kuril Islands earthquakes, *Geophys. Res. Lett., 22,* 2297-3000, 1995.

Van der Hilst, R. D., S. Widiyantoro, and E. R. Engdahl, Evidence for deep mantle circulation from global tomography, *Nature, 386,* 578-584, 1997.

Vasco, D. W.,, and L. R. Johnson, Whole earth structure estimated from seismic arrival times, *J. Geophys. Res., 103,* 2633-2671, 1998.

Widiyantoro, S., B. L. N. Kennett, and R. D. Van der Hilst, Joint Seismic Tomography for Three-Dimensional Shear and Bulk-Sound Velocity Structure in the Mantle, paper presented at 29th General Assembly, IASPEI, Thessaloniki, Greece, August 18-28, 1997.

Widmer, R., G. Masters, and F. Gilbert, Observably split multiplets - data analysis and interpretation in terms of large-scale aspherical structure, *Geophys. J. Int., 111,* 559-576, 1992.

Woodhouse, J. H., The coupling and attenuation of nearly resonant multiplets in the Earth's free oscillation spectrum, *Geophys. J. R. Astron. Soc., 61,* 261-283, 1980.

J. S. Resovsky and M. H. Ritzwoller, Department of Physics, University of Colorado, Boulder CO 80309-0390. (resovsky@abdu.colorado.edu)

(Received May 6, 1998; revised September 10, 1998; accepted September 11, 1998.)